Graduate School Form 30
(Revised 08/14)

PURDUE UNIVERSITY
GRADUATE SCHOOL
Thesis/Dissertation Acceptance

This is to certify that the thesis/dissertation prepared

By Jing Li

Entitled
MODELING AND ANALYSIS OF AN AIR HANDLING UNIT TO IMPROVE ENERGY EFFICIENCY

For the degree of Master of Science in Mechanical Engineering

Is approved by the final examining committee:

Jie Chen

David Goodman

Ali Razban

To the best of my knowledge and as understood by the student in the Thesis/Dissertation Agreement, Publication Delay, and Certification/Disclaimer (Graduate School Form 32), this thesis/dissertation adheres to the provisions of Purdue University's "Policy on Integrity in Research" and the use of copyrighted material.

Jie Chen

Approved by Major Professor(s): _____

_____

Approved by: Sohel Anwar 06/25/2015

Head of the Department Graduate Program Date

MODELING AND ANALYSIS OF AN AIR HANDLING UNIT TO IMPROVE ENERGY EFFICIENCY

A Thesis

Submitted to the Faculty

of

Purdue University

by

Jing Li

In Partial Fulfillment of the

Requirements for the Degree

of

Master of Science in Mechanical Engineering

August 2015

Purdue University

Indianapolis, Indiana

To My Parents

ACKNOWLEDGMENTS

I would like to express my deepest gratitude to my advisor Dr. Jie Chen for his excellent guidance, extensive knowledge, patience, and providing me continuous support and motivation to complete my research and write the thesis.

Many thanks and appreciation to my thesis committee, Dr. David Goodman and Dr. Ali Razban, for their insightful comments, encouragements and constant support throughout my research.

I will be forever thankful to Mr. Tom Pennington. Without his inspirations and generously sharing his knowledge with me, I would never have been able to finish my thesis.

Sincere thanks to Xinye Zhang, who as a good friend, has shared his extensive knowledge in using Engineering Equation Solver with me. I would also like to thank Terry Cohoat, Vince Cohoat, Madelynn Dowdy Moody and Brad Powell for helping and supporting me in numerous ways for the past several months.

Special thanks to my company, Carrier Corporation. Without the flexible schedules and financial support, it would have made my research so much harder to accomplish.

Thanks IAC members for providing continuous support throughout the thesis.

Finally, I would like to express my heartfelt gratitude to my parents and my brother in China. Words cannot express my love and appreciation to you. Thanks for continuously supporting me throughout my life. Without you and your love, my dreams would have not come true.

TABLE OF CONTENTS

Page

LIST OF TABLES vi

LIST OF FIGURES vii

SYMBOLS ix

ABBREVIATIONS xii

ABSTRACT xiii

1. INTRODUCTION 1
   1.1 Problem Statement 1
   1.2 Literature Review 3
      1.2.1 Modeling Approaches 4
      1.2.2 HVAC Simulation Tools 7
   1.3 General Research Objectives 8
   1.4 Thesis Outline 8

2. METHODOLOGY 10

3. EXPERIMENTS AND DATA COLLECTION 12
   3.1 Experiment Goals 12
   3.2 Test Facility 12
   3.3 Floor Layout 12
   3.4 HVAC System 12
   3.5 Air Handling Unit 14
   3.6 AHU Design Specifications 14
   3.7 VAV Terminal Unit Specifications 14
   3.8 Building Automation System 15
      3.8.1 AHU I/O List 18
      3.8.2 Sensor Types 18
      3.8.3 Sensor Locations 18
   3.9 AHU Sequence of Operation 18
      3.9.1 Air Handling Unit Start/Stop 18
      3.9.2 Duct Static Pressure Control 20
      3.9.3 Preheat Coil Controll 20
      3.9.4 Mixed Air Temperature Control 21
      3.9.5 Carbon Dioxide Control (Demand Control Ventilation/DCV) 21
      3.9.6 Economizer/Mixed Air Damper Control 21

Page
3.9.7 Cooling Coil Control . . . 22
3.9.8 Heating warm-up (Transition for Unoccupied to Occupied only) 23
3.9.9 Cooling Pull-Down (Transition from Unoccupied to Occupied only) . . . 23
3.9.10 Safeties . . . 23
3.9.11 Cooling Coil Recirculation Pump Control . . . 24

4. MATHEMATICAL MODELING . . . 28
4.1 Mixing Box Model . . . 30
4.2 Supply Fan Model . . . 33
4.3 Temperature Rise Across Supply Fan Model . . . 34
4.4 Return Fan Model . . . 34
4.5 Preheat Coil Model . . . 35
4.6 Cooling Coil Model . . . 37
4.7 Zone Model . . . 38

5. RESULTS AND VALIDATIONS . . . 40
5.1 AHU Model Validation . . . 40
5.1.1 Mixing Box Model Validation . . . 40
5.1.2 Supply Fan Model Validation . . . 42
5.1.3 Return Fan Model Validation . . . 44
5.1.4 Preheat Coil Model Validation . . . 48
5.1.5 Cooling Coil Model Validation . . . 49
5.2 Error Rate Analysis . . . 49
5.3 Baseline Energy Consumption . . . 51

6. UNCERTAINTY ANALYSIS . . . 52

7. CONTROL STRATEGY OPTIMIZATION . . . 56
7.1 Discharge Air Temperature Reset . . . 56
7.2 Static Pressure Reset . . . 56
7.3 Potential Energy Saving Prediction . . . 59

8. DISCUSSIONS . . . 62

9. CONCLUSIONS AND RECOMMENDATIONS . . . 63
9.1 Conclusion . . . 63
9.2 Recommendations for Future . . . 63

LIST OF REFERENCES . . . 65

LIST OF TABLES

Table		Page
3.1	AHU design specifications [22]	15
3.2	VAV terminal unit specifications [23]	25
3.3	AHU I/O list	26
3.4	Sensor types installed on the AHU [22]	27
5.1	Description of data sets for model validation	40
5.2	Error differences comparison for individual model	51
5.3	Baseline energy consumption	51
7.1	Description of data sets for energy consumption comparison	60
7.2	Energy savings comparison between DA-T reset and SP reset	60

LIST OF FIGURES

Figure		Page
1.1	Commercial sector energy end-use distribution [1]	1
1.2	Typical Heating, Ventilation and Air Conditioning system [4]	2
1.3	Black box approach schematic [10]	5
1.4	White box approach schematic [15]	6
1.5	General data flow of simulation engines [18]	7
2.1	Methodology flowchart	10
3.1	Facility floor layout [21]	13
3.2	AHU schematic diagram	14
3.3	BAS network architecture [25]	16
3.4	Sensor locations on the AHU	19
3.5	Carbon Dioxide Control flowchart	22
4.1	Major energy consumers of HVAC system	28
4.2	Inputs and outputs of the AHU model	29
4.3	Mixing box schematic diagram [27]	30
4.4	Mixing air damper control flowchart	31
4.5	Mixing box model logic	32
4.6	Supply fan model logic	34
4.7	Return fan model logic	35
4.8	Schematic diagram of the pre-heat coil	36
4.9	Schematic diagram of the cooing coil	38
4.10	Components of a VAV box [36]	39
5.1	Calculated MA-T vs. Actual MA-T (2/1/2015-2/28/2015)	41
5.2	MA-T Error vs. OAT (2/1/2015-2/28/2015)	41
5.3	Calculated MA-T vs. Actual MA-T (3/1/2015-3/31/2015)	42

Figure Page

5.4 Calculated supply fan power vs. measured supply fan power (2/1/2015-2/28/2015) . . . 43

5.5 Correlation between measured supply fan power and predicted supply fan power . . . 43

5.6 Calculated supply fan power vs. measured supply fan power (3/1/2015-3/31/2015) . . . 44

5.7 Actual vs. Simulated return fan power (2/1/2015-2/28/2015) . . . 45

5.8 Actual vs. Simulated return fan power (3/1/2015-3/31/2015) . . . 45

5.9 Correlations between calculated and actual return fan power . . . 46

5.10 Actual return fan power vs. Simulated return fan power after calibration (2/1/2015-2/28/2015) . . . 46

5.11 Actual return fan power vs. Simulated return fan power after calibration (3/1/2015-3/31/2015) . . . 47

5.12 Calculated PH-T vs. Actual PH-T (2/1/2015-2/28/2015) . . . 47

5.13 Calculated PH-T vs. Actual PH-T (3/1/2015-3/31/2015) . . . 48

5.14 Calculated DA-T vs. Actual DA-T (2/1/2015-2/28/2015) . . . 49

5.15 Calculated DA-T vs. Actual DA-T (3/1/2015-3/31/2015) . . . 50

6.1 Uncertainty propagation . . . 53

6.2 Uncertainties of measured variables . . . 54

6.3 Uncertainty results . . . 54

7.1 Discharge air temperature reset logic . . . 57

7.2 Correlation between DA-T and RA-T in DA-T reset logic . . . 58

7.3 Supply air static pressure reset logic . . . 59

SYMBOLS

c	Overall thermal capacity
$c_{p,ma,c}$	Mixed air specific heat
$c_{p,cw}$	Chilled water specific heat
$c_{p,hw}$	Hot water specific heat
$CF_{min,hr}$	Conversion factor
BHP_{SF}	Supply fan motor horsepower
BHP_{RF}	Return fan motor horsepower
E_{SF}	Supply fan energy consumption
E_{RF}	Return fan energy consumption
h_{oa}	Outside air enthalpy
h_{ra}	Return air enthalpy
h_{ea}	Exhaust air enthalpy
h_{ma}	Mixed air enthalpy
h_{DA}	Discharge air enthalpy
PLR_{sf}	Supply fan part load ratio
PLR_{rf}	Return fan part load ratio
Q_{hw}	Preheat coil energy consumption
Q_{cc}	Cooling coil energy consumption
Q_{rh}	Reheat coil energy consumption
Q_{total}	Total energy consumption
RH_{oa}	Outside air relative humidity
RH_{ra}	Return air relative humidity
ρ_{oa}	Outside air density
ρ_{ra}	Return air density
ρ_{ea}	Exhaust air density

ρ_{ma}	Mixed air density
ρ_{hw}	Hot water density
ρ_{cw}	Chilled water density
t	Sampling interval
T_{oa}	Outside air temperature
T_{ra}	Return air temperature
T_{ea}	Exhaust air temperature
T_{ma}	Mixed air temperature
T_{DA}	Discharge air temperature
$T_{ma,c}$	Corrected mixed air temperature after supply fan
$T_{hw,i}$	Preheat coil inlet hot water temperature
$T_{hw,o}$	Preheat coil outlet hot water temperature
$T_{ao,ph}$	Preheat coil outlet air temperature
$T_{cw,i}$	Cooling coil inlet chilled water temperature
$T_{cw,o}$	Cooling coil outlet chilled water temperature
$T_{a,i}$	Cooling coil inlet air temperature
$T_{a,o}$	Cooling coil outlet air temperature
ΔT_{SF}	Temperature rise across supply fan
UA_{hw}	Preheat coil Overall heat transfer coefficient
UA_{cc}	Cooling coil Overall heat transfer coefficient
$\dot{V}_{oa}$	Outside air flow rate
$\dot{V}_{ra}$	Return air flow rate
$\dot{V}_{ea}$	Exhaust air flow rate
$\dot{V}_{sa}$	Supply air flow rate
$\dot{V}_{sf,design}$	Design supply air flow rate
$\dot{V}_{rf,design}$	Design return air flow rate
$\dot{V}_{hw}$	Hot water flow rate
$\dot{V}_{cw}$	Chilled water flow rate
$\dot{W}_{SF,btuhr}$	Supply fan power

X_{oa}	Outside air humidity ratio
X_{ra}	Return air humidity ratio
X_{ea}	Exhaust air humidity ratio
X_{ma}	Mixed air humidity ratio

ABBREVIATIONS

ADS	Application and Data Server
AHU	Air Handling Unit
ANN	Artificial Neutral Network
BAS	Building Automation System
CCT	Controller Configuration Tool
DDC	Direct Digital Control
DCV	Demand Control Ventilation
EES	Engineering Equation Solver
EMS	Energy Management System
FEC	Field Equipment Controller
GA	Genetic Algorithm
MAPE	Mean Absolute Percentage Error
MLR	Multiple Liner Regression
NAE	Network Automation Engine
NCE	Network Controller Engine
NIE	Network Integration Engine
PI	Proportional Integral
PID	Proportional Integral Derivative
PLR	Part Load Ratio
RSMD	Root Square Mean Deviation
RSS	Root Sum Square
SCT	System Configuration Tool
VAV	Variable Air Volume
VFD	Variable Frequency Drive

ABSTRACT

Jing, Li. M.S.M.E., Purdue University, August 2015. Modeling and Analysis of an Air Handling Unit to Improve Energy Efficiency. Major Professors: Jie Chen and David Goodman.

The Air Handling Unit (AHU), which serves the entire basement of Engineering and Technology (ET) building on IUPUI campus, had constant set points of discharge air temperature and supply air static pressure. Two reset schedules were investigated to determine which was the best control strategy to minimize energy consumption of the AHU.

In this research, a gray box model was established to create the baseline of energy consumption with constant set points and predict the energy savings using two different reset schedules. The mathematical model was developed in Engineering Equation Solver (EES). It was validated using two sets of sub hourly real time data. The model performance was evaluated employing Mean Absolute Percentage Error (MAPE) and Root Mean Square Deviation (RMSD).

Additionally, uncertainty propagation identified outside air temperature, supply airflow rate and return air temperature were the key parameters that had an impact in overall energy consumption.

Discharge air temperature was reset based on return air temperature (RA-T) with a linear reset schedule from March 4 to March 7. Static pressure was reset based on the widest open Variable Air Volume (VAV) box damper from March 20 to March 23. Results indicated that 17% energy savings was achieved using discharge air temperature reset while the energy consumption reduced by 7% using static pressure reset.

1. INTRODUCTION

1.1 Problem Statement

Residential and commercial buildings account for 41% of total energy consumption [1] and 39% of carbon dioxide (CO_2) emissions in the United States [2]. Primary building energy end use include lighting, space heating, space cooling, water heating, ventilation, etc. [3]. As shown in Figure1.1, Heating, Ventilation and Air-conditioning (HVAC) systems are the largest energy consumer, accounting for 32% of total building energy use [3].

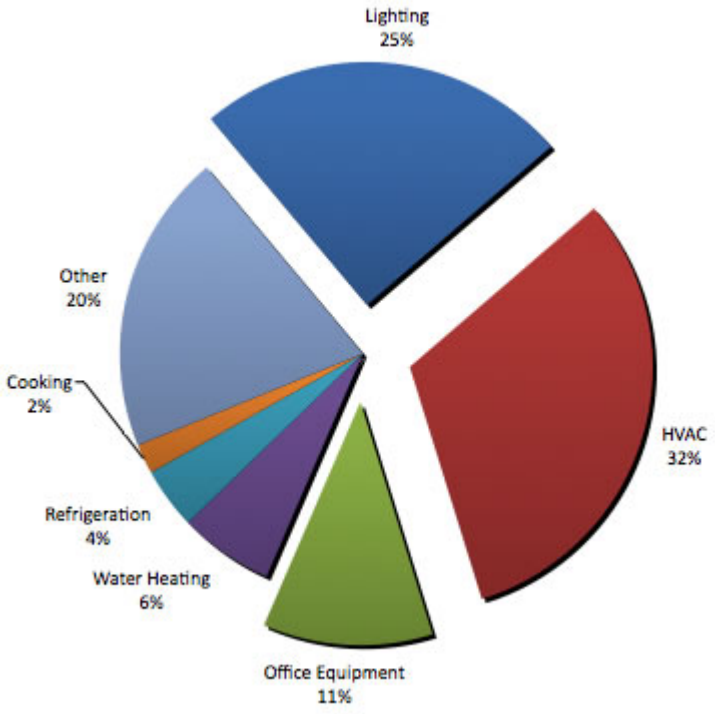

Figure 1.1. Commercial sector energy end-use distribution [1]

The primary energy source consumed in the United States comes from fossil fuel [1]. The combustion of fossil fuel makes a major contribution to global warming, which is one of the most significant environmental issues of our time. Thus, it is essential to improve the energy efficiency of HVAC systems to reduce energy usage and minimize the negative effects on environment.

A typical HVAC system consists of a central heating plant, a central cooling plant, air handling units, air distribution system, terminal units and energy management system. See Figure 1.2.

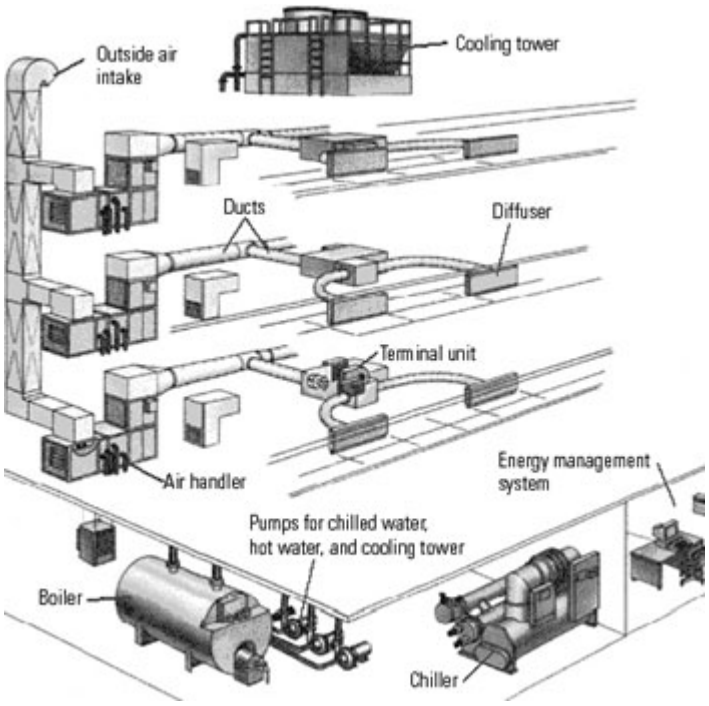

Figure 1.2. Typical Heating, Ventilation and Air Conditioning system [4]

There are potential energy saving opportunities for each element. However, chilled water and hot water were provided by Citizen Energy Group for IUPUI HVAC systems. The chillers and boilers were not accessible. Due to accessibilities to facility and data collection system, this research focused on an AHU on the IUPUI campus. The facility information will be demonstrated in Chapter 3.

The targeted AHU is located in the ET building basement. The AHU operates as follows: a portion of return air and outside air mix together in the mixing chamber. The mixed air is delivered via supply fan to be conditioned. The supply fan speed is modulated to maintain the duct static pressure, which was set at 1.80 in. WC to overcome the total pressure loss along the duct downstream and the pressure drop in the terminal units. The outlet temperature of the cooling coil is discharge air temperature (DA-T). It was set at a constant value of 55°F.

Constant setpoints of discharge airtemperature and supply air static pressure contribute to significant energy waste. ASHRAE Standard 90.1-2010 requires multi-zone HVAC systems to implement supply air temperature reset. It is also mandatory to conduct static pressure reset schedules for systems with Direct Digital Control (DDC) of individual VAV boxes reporting to the central control panel.

1.2 Literature Review

A few studies have been conducted with regards to the reset schedules. Li et al. [5] presents that significant energy savings were achieved by optimizing the supply air temperature in a variable air volume system in different climates. A steady state energy consumption model of a single zone VAV AHU system was developed in Zhou et al. [6], the supply air temperature was optimized using analytical optimization method to minimize the energy usage during economizer operation. In this study, estimated 90% energy was saved under specific space loads and outside air condition. However, the simulated results and control sequence were not validated through experiments.

As for static pressure reset control strategy, Liu et al. [7] presented that fan power consumption and thermal energy consumption including both heating and cooling decreased with static pressure reset strategy. Housholder et al. [8] employed Proportional plus Integral (PI) control loops and Tier and Respond static pressure reset strategies at the Energy Resource Station to make a comparison on the energy savings.

Housholder et al. [8] implemented the strategy that led to the most substantial energy savings on the Lowe State University campus. The test results demonstrated that the tiered Trim and Respond reset strategy contributed to 37% fan energy savings per week.

Above studies provide good indications that reset schedules could reduce energy consumption of HVAC systems. However, the studies did not draw a comparison of the energy savings using different reset strategies. Additionally, no models were developed in the studies to predict the potential energy savings.

Modeling is the key in predicting system operation and performance. Three types of analytical approaches, known as white box, black box and gray box approach, have been widely used for HVAC systems modeling [9]. Black box model is data driven and mainly used for fault detection of an existing system. The generalization capability of a black box model is relatively low without knowing the system details. White box model is physics-based and primarily adopted for optimal design. However, due to complexity of HVAC systems, it is probably impossible to establish a solid model in reasonable time employing the white box modeling technique. Gray box modeling is a combination of both. The system configuration is not entirely known for gray box model. However, a number of parameters can be estimated based on the relationship between inputs and outputs. The relationship is obtained through the system and experimental data [9]. Thus, gray box modeling technique was adopted in this research.

1.2.1 Modeling Approaches

Black Box Approach (Data-Driven Approach)

Black box analytic method, also known as data driven approach, has been used widely in HVAC industry. The black box aproach schematic is displayed in Figure 1.3. Performance data of an HVAC system is gathered under different operation conditions. Mathematical models, such as simple or multiple linear regression and

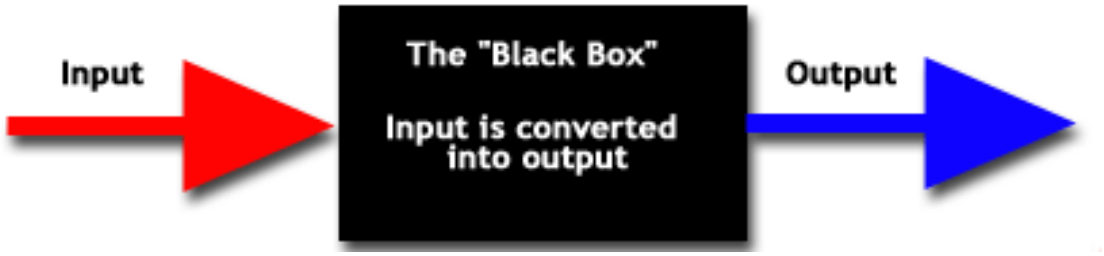

Figure 1.3. Black box approach schematic [10]

Artificial Neutral Network (ANN), are used to establish the relationship between measured input parameters and output parameters without knowing the internal structure of the system [9].

The advantage of black box approach is that it is comparatively simpler to use and also more accurate to predict the future system performance of an existing HVAC system [9]. A few researches have been developed using data-driven method. Kalogirou et al. [11] demonstrated how ANNs and Genetic Algorithm (GA) contributed to the modeling and prediction of the performance of a wide variety of energy systems. Katipamula et al. [12] used multiple linear regression (MLR) methodology to model the cooling energy consumption of 5 commercial buildings on different time scales. Kusiak et al. [13] employed data mining algorithms to develop dynamic models for mapping out input and output variables of an air handling unit in order to reduce the cooling energy consumption.

Although data-driven approach can accurately predict the performance for a given HVAC system, the generalization capability is relatively low since underlying physical principles and system interactions are unknown [9, 14].

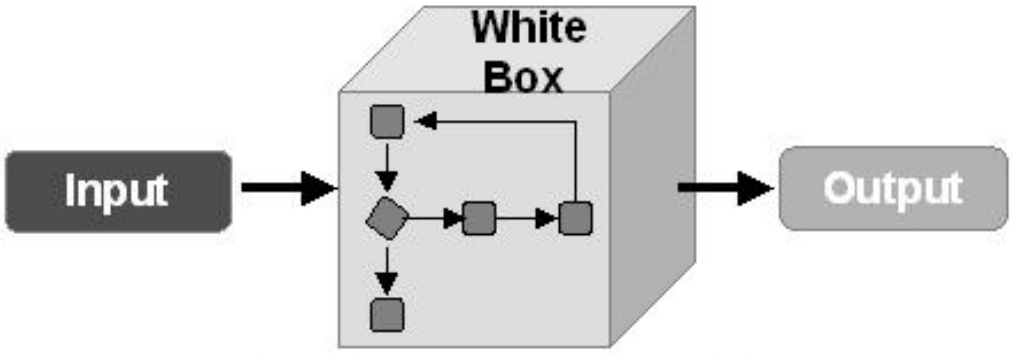

Figure 1.4. White box approach schematic [15]

White Box Approach (Forward Approach)

In contrast to data-driven approach, the outputs of the system models can be predicted having the detailed knowledge of the target system structure and specified input parameters as shown in Figure 1.4. In terms of the accuracy of the HVAC modeling, it is essential to know how the variables affect system behaviors [14]. The physics-based models are created by using governing equations.

The major benefit of white box approach is that it does not need to set up a complex physical system to predict system behavior [14]. It eliminates a large amount of physical setup, which drastically reduces the design and operation costs. A dynamic model of an HVAC system including a zone, heating coil, cooling and dehumidifying coil, humidifier, ductwork, fan and mixing box was derived using energy and mass balance governing equations for control optimization [16].

White box modeling requires detailed knowledge about internal structure and physical configuration of the building or the HVAC system [14]. With regards to retrofit projects, the details of building envelope characteristics and equipment characteristics are usually hard to obtain. Assumptions can be made to perform forward modeling. Calibration process plays an important role in improving the accuracy of the simulated model by utilizing field measured data.

Gray Box Approach

Gray box method is a combination of physical and non-physical approaches. Primarily, a physical model is developed to illustrate the system configuration and underlying process. And then key variables that have a substantial influence on system performance are identified [14].

Gray box approach has an advantage over the other two approaches due to its accurate prediction of system output and respectively high generalization capability by utilizing both physics equations and field measured data [17]. This approach can be potentially used in fault detection and diagnosis (FDD) [14].

1.2.2 HVAC Simulation Tools

HVAC system simulation can be conducted in the building energy performance simulation tools, such as DOE-2, EnergyPlus, eQuest, TRNSYS etc. Figure 1.5 shows the general data flow of simulation engines.

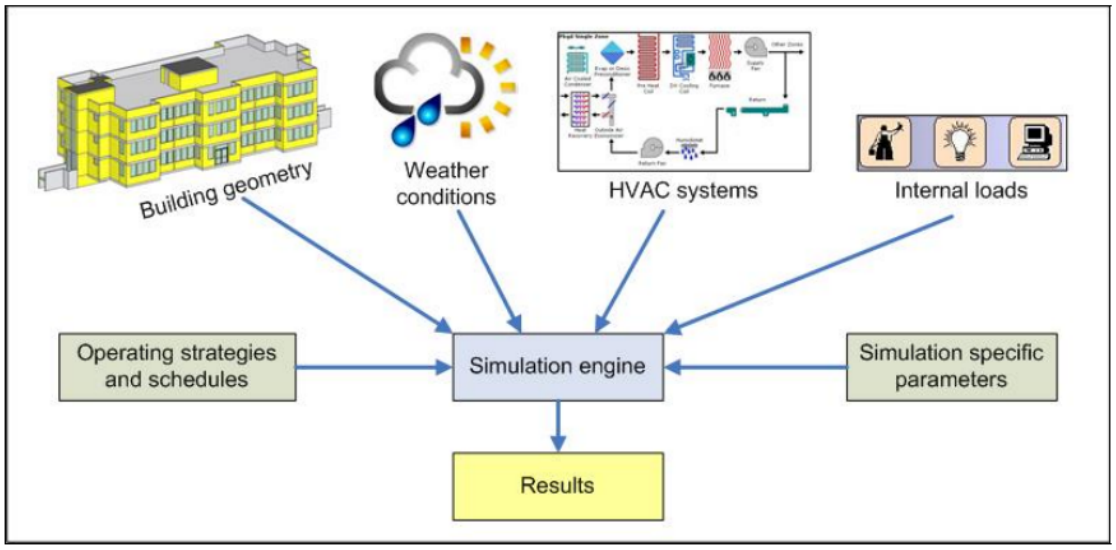

Figure 1.5. General data flow of simulation engines [18]

The current HVAC simulation programs include comprehensive transient models for heating and cooling loads under different operating conditions using white box modeling approach. However, they do not have the full flexibilities to customize advanced PID controllers in a complex HVAC system [17, 19].

HVAC system simulation can also be performed in some other software, such as MATLAB Simulink, Engineering Equation Solver (EES), Dymola, etc. Afram et al. [17] developed transient models of residential HVAC system in MATLAB Simulink and precisely predict the output parameters. However, MATLAB Simulink does not provide the units of measurement, built-in thermodynamic and transport properties, and uncertainty analysis and propagation, which makes the simulation more complicated for complex HVAC systems [20]. Therefore, EES was used in this project due to its capabilities to import thermodynamic and transport properties from REFPROP and also provide the units of measurements.

1.3 General Research Objectives

The goal is to optimize the energy consumption of an air handling unit (AHU) without compromising the industrial standards. The primary objectives of this research were to optimize the energy consumption of an air handling unit in an academic building on campus through system modeling. The research aims to (1) develop and validate a mathematical model, which can be used to predict the system performance and energy consumption, and (2) to recommend measures for optimizing the AHUs performance. It is expected that methodologies can be applied to other energy consuming equipment.

1.4 Thesis Outline

This thesis is divided into eight chapters. Chapter 1 provides the background information of the problem that will be addressed in this paper. An overview of modeling approaches, simulation tools and control strategies is also included. Chapter 2

describes the methodology that will be utilized to solve the problem stated in Chapter 1. Chapter 3 demonstrates the tested facility, HVAC components specifications, data collection system and AHU sequence of operation. Chapter 4 shows the mathematical model of each AHU component using energy and mass energy balance equations. In Chapter 5, the theoretical model is validated by a comparison with real time data. The deviations between simulated data and measured data are analyzed employing MAPE and RSME. Additionally, the baseline of energy usage is created using constant supply air static pressure and discharge air temperature setpoints. Chapter 6 shows the key parameters that have great influences in energy consumption are determined by using uncertainty analysis in EES. Reset control strategies are illustrates in Chapter 7. In addition, energy consumption comparison between baseline model and optimized model is demonstrated. Chapter 8 discusses the results and identifies the potential opportunities for future work.

2. METHODOLOGY

The main objective of this project was to optimize energy consumption and decrease operational costs of an AHU on campus. Figure 2.1 shows the methodology used in this study. The details are demonstrated in the following chapters.

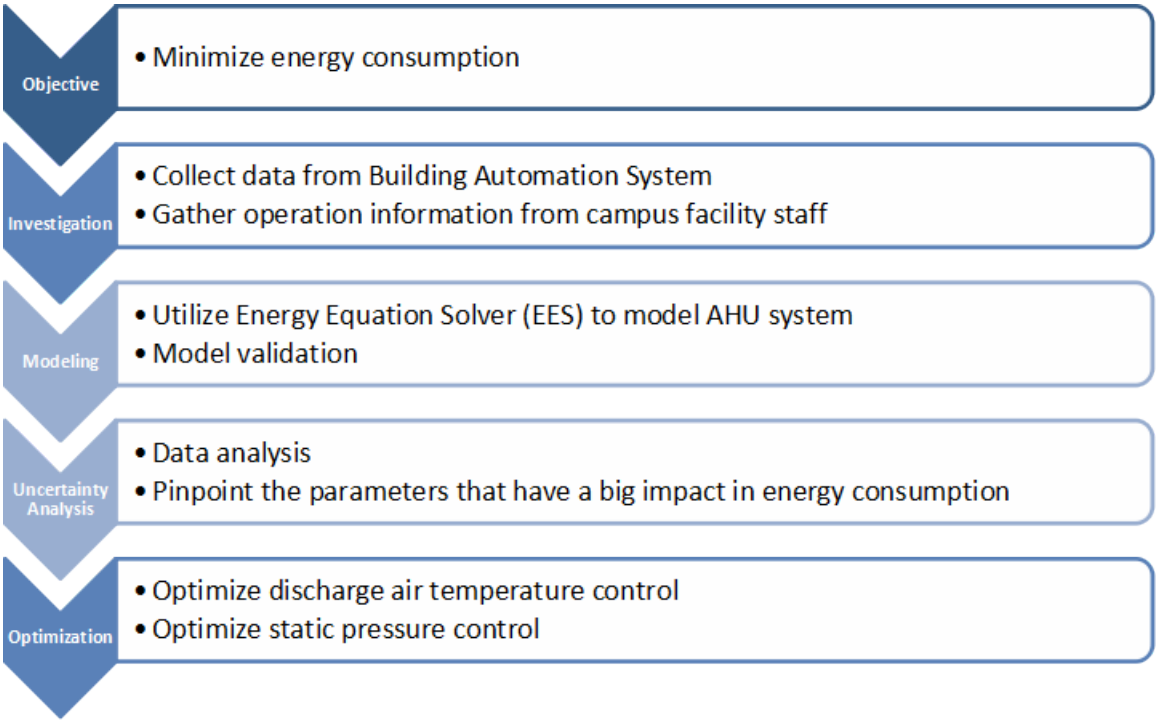

Figure 2.1. Methodology flowchart

Relevant data was collected during investigation stage. Sensors and flow stations had already been installed on the AHU to monitor the key parameters (temperature, humidity, static pressure, airflow, etc.). The data was then filtered and transferred to Building Automation System (BAS). Some of the inputs and outputs were selected

for model simulation. In addition, operation information and design specifications of the AHU were gathered from Campus Facility Staff at this stage.

The AHU consists of a supply fan, a return fan, a cooling coil, a preheat coil and terminal units. Individual component was modeled using energy and mass balance governing equations that represent the inherent physical processes and interactions with other components. Engineering Equation Solver (EES) was selected for system simulation due to its capabilities of finding the solutions of a large set of complicated equations. EES is allowed to import thermodynamic and transport properties from REFPROP. It is also able to solve engineering problems associated with other programs using dynamic data exchange [20].

The mathematical model needed to be validated after it was developed. Model validation played an essential role to ensure the reliabilities of the AHU system model in terms of energy performance prediction. The simulated outputs and energy consumption of each component were compared with measured data and energy usage using real time data as inputs. Mean Absolute Percentage Error (MAPE) and Root Mean Square Deviation (RMSD) for individual components were evaluated to illustrate model performance.

Uncertainly analysis was performed to pinpoint the parameters that had significant influence in energy consumption. The key parameters could be controlled and optimized to reduce the overall energy consumption and energy costs for future study.

3. EXPERIMENTS AND DATA COLLECTION

3.1 Experiment Goals

The main goal of the experiments was to validate the mathematical model developed in the Chapter 4 by comparing real time data with simulated data.

3.2 Test Facility

Testing was conducted in the basement of ET Building on IUPUI campus. The construction was completed in 2006. The total square footage of the ET basement is 31,957 square feet. The primary use of the basement is classrooms. It also includes labs, general study area and mechanical room.

3.3 Floor Layout

The floor layout is shown in Figure 3.1.

3.4 HVAC System

An HVAC system provides thermal comfort and maintains indoor air quality to a building. It includes maintaining appropriate temperature and humidity level, improving the indoor air quality by taking in fresh outside air and removing the air contaminants from/to the conditioned area.

The central heating plant on campus provides hot water to the entire HVAC system of ET building, including the preheat coils in different air handling units and the reheat coils in the terminal units. The central cooling plant delivers the chilled water to the cooling coils of various AHUs. In cooling operation, chilled water from

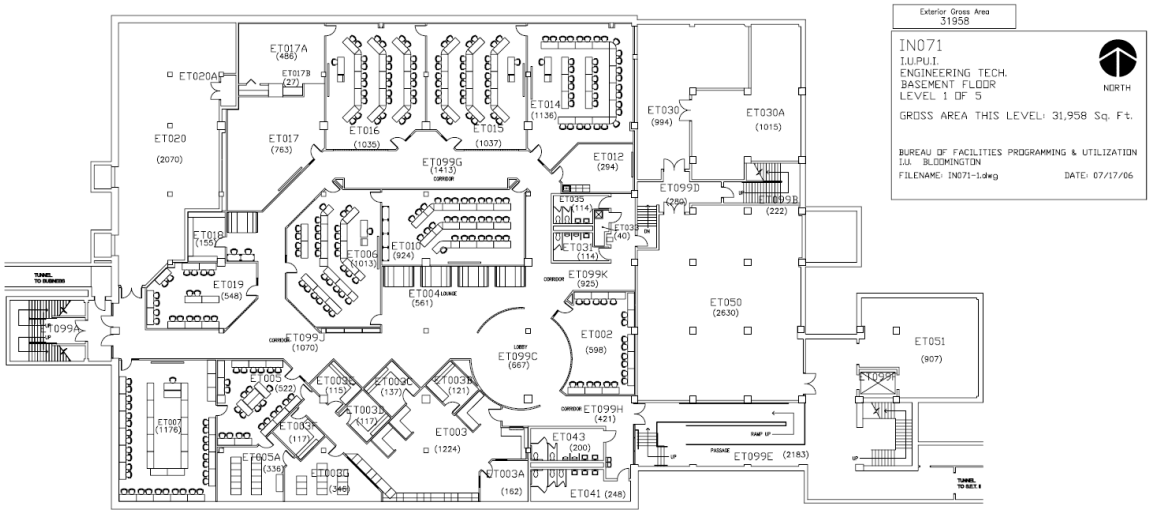

Figure 3.1. Facility floor layout [21]

the central cooling plant removes the heat and moisture from the indoor environment. In heating operation, hot water from the central heating plant provides the heat to the conditioned space.

Building ventilation is provided by the air handling unit. The fresh outside air is drawn in through a supply fan and mixes with a portion of return air in the mixing chamber. The mixed air is filtered, conditioned and then distributed to the conditioned space via air ducts. Terminal units reheat the conditioned air to meet the desired room temperature. The conditioned air is discharged through the air diffusers to different zones.

An Energy Management System (EMS), sometimes called Building Automation System (BAS), is used to monitor and control the HVAC, security, fire, and lighting systems of a building to reduce the operational cost and optimize the building performance.

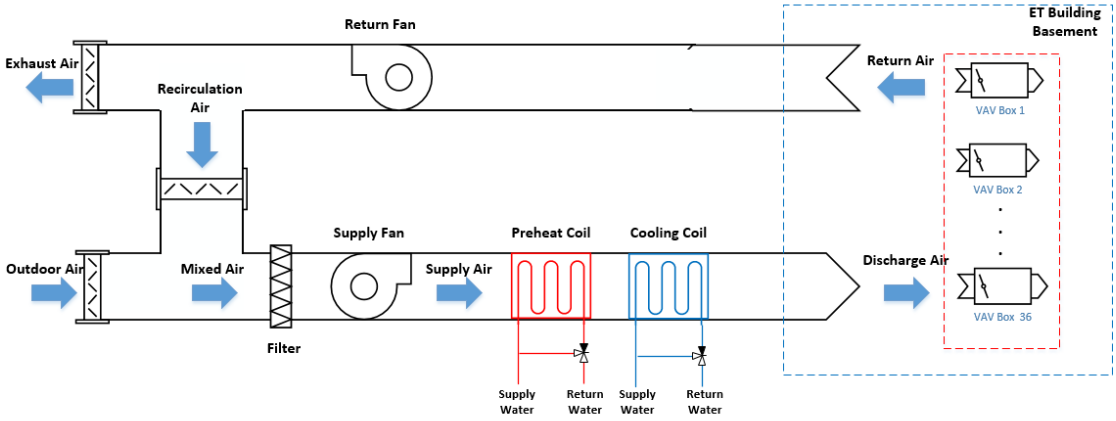

Figure 3.2. AHU schematic diagram

3.5 Air Handling Unit

In tested facility, one Variable Air Volume (VAV) Air Handling Unit with an interlocked supply fan, return fan, hot water coil, chilled water coil and a full economizer, serving 36 VAV Single-Duct pressure independent terminal units throughout the ET basement. Figure 3.2 displays the AHU schematic diagram.

3.6 AHU Design Specifications

Table 3.1 describes the AHU design specifications.

3.7 VAV Terminal Unit Specifications

All 36 VAV boxes are pressure independent. Individual terminal box is equipped with a flow sensor to limit the airflow setpoint between the minimum and maximum flow setting [23]. The supply air temperature and static pressure are controlled

Table 3.1. AHU design specifications [22]

Components	**Specifications**	
Preheat Coil	Surface Area:	40 sq. ft
	Rows:	1
	MBH (Mega BTU per hour):	733
Cooling Coil	Surface Area:	40 sq. ft
	Rows:	6
	MBH (Mega BTU per hour):	796
Supply Fan	Min OA CFM:	5000
	Supply CFM:	17000
	Horsepower:	25
	External Static Pressure:	3 in. WC
Return Fan	Supply CFM:	17000
	Horsepower:	15
	External Static Pressure:	1.75 in. WC

by DX9100 controller while each thermal zone has its local controller.The technical information of the terminal units are described in Table 3.2.

3.8 Building Automation System

The ET buildings building automation system employs Johnson Controls Metasys building management system. Strong interoperability and improved wireless performance enable Metasys to provide full integration of numerous pieces of equipment and subsystems, from HVAC systems to lighting, from security to fire systems. With availabilities of data collection and trend analysis, operators are able to improve overall efficiency and productivity of the facility [24].

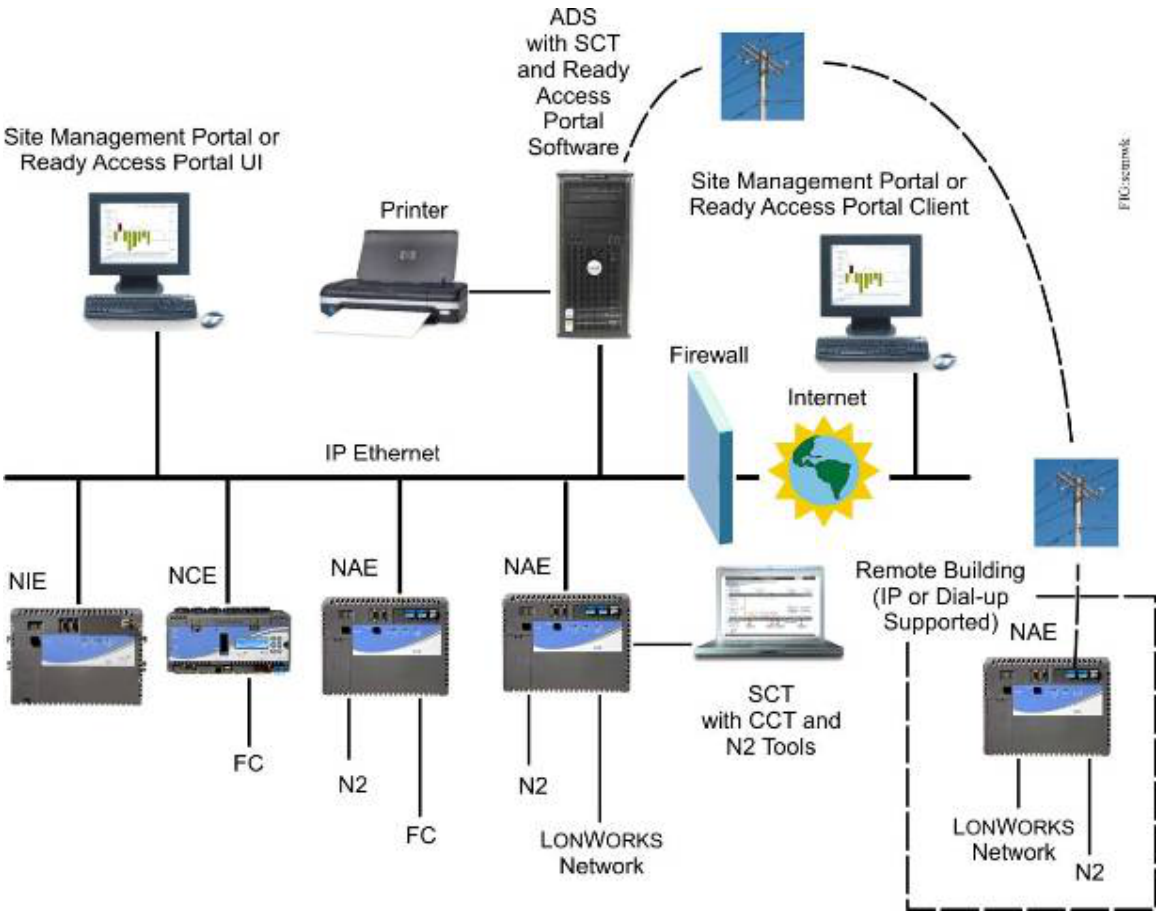

Figure 3.3. BAS network architecture [25]

Metasys interacts with local Field Equipment Controller (FEC) via a series of network commands. The BAS shares global information, including operator-entered commands that cannot otherwise be seen by the local FEC [25].

The architecture components and communication structure of Metasys discussed below are shown in Figure 3.3.

Network Automation Engine (NAE)

The NAE is a supervisory controller that comprehensively monitors and supervises a wide variety of HVAC equipment, lighting, security, and fire safety devices through IP network connectivity and web-based access to BAS [25].

Network Integration Engine (NIE)

The NIE is a specialized version of NAE to integrate N1 networks or Honeywell Excel 5000 systems [25].

Network Controller Engine (NCE)

The Network Controller Engine (NCE) controllers integrate NAE with the Input/Output (I/O) point capabilities and the functionalities of DDC of a wide range of FECs [25].

Application and Data Server (ADS)

The ADS is a Metasys server to archive the historical data for trend analysis, alarm and event data [25].

System Configuration Tool (SCT)

SCT is used for offline configuration of Metasys system engines which allows operators to create archive databases that can be downloaded to an Engine or Server [25].

Controller Configuration Tool (CCT)

The CCT provides configuration, simulation, and commission to the field equipment controllers, Input/Output modules and VAV modular Assembly [25].

Metasys N2

Metasys N2 protocol allows third party devices to be integrated into BMS [25].

3.8.1 AHU I/O List

Table 3.3 shows the inputs and outputs of the AHU that serves the ET basement. Some of the inputs and outputs were used for simulation.

3.8.2 Sensor Types

Sensor types installed on the AHU are shown in Table 3.4. Averaging temperature sensors have been used to measure CHR-T, MA-T, PH-T and DA-T.

3.8.3 Sensor Locations

Sensor locations are displayed in Figure 3.4.

3.9 AHU Sequence of Operation

The sequences of operation [26] show how AHU operates over different operating phases (warm-up, occupied, unoccupied).

3.9.1 Air Handling Unit Start/Stop

The unit shall run continuously in the occupied mode and cycle in the unoccupied mode to maintain the lowest space temperature above a setback temperature of 60°F in the heating season. The occupied cycle will be selected at the electronic control system operators workstation through the Building Management System via an electronic time schedule.

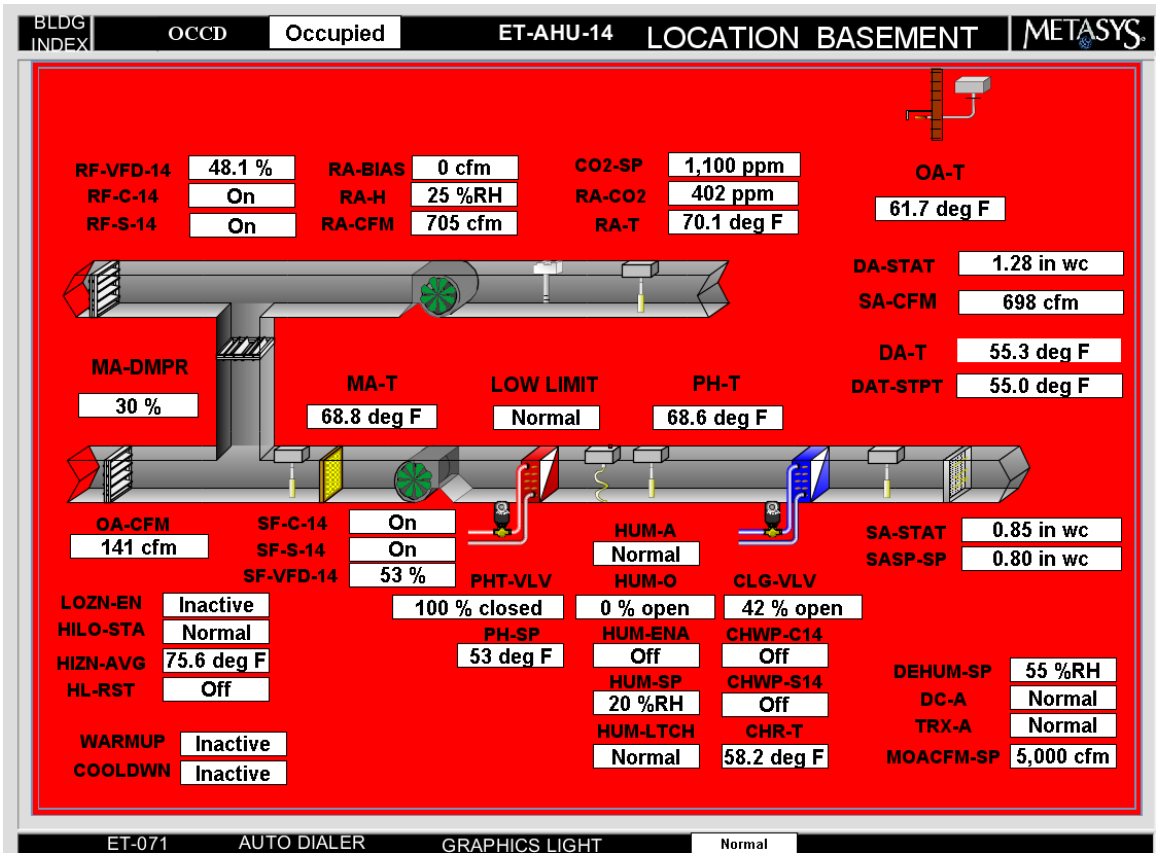

Figure 3.4. Sensor locations on the AHU

When the unit is stopped, outside air dampers (MA-DMPR) will close, return air dampers (RA-DMPR) will open, chilled water control valve (CLG-VLV) closes, the variable frequency drives (SF-VFD1, RF-VFD1) ramp down and the preheat coil control valve (PHT-VLV) maintains an inside the casing temperature of 50°F. Outside air dampers are to remain closed during unoccupied operation.

3.9.2 Duct Static Pressure Control

The duct static pressure (SA-STAT) will be maintained by modulating the supply fan (SF-VFD1) speed through the variable frequency drive (SF-VFD1). The VFD is controlled to maintain a 2/3 downstream duct static (SA-STAT) setpoint of 1.80 WC. downstream duct static (SA-STAT) will control the VFD through the application specific controller (DC-1). An electric static pressure hi-limit safety device (HI-STAT) will stop the supply fan whenever fan discharge static pressure rises above the 4.5 WC high limit. The electric static pressure hi-limit switch will be equipped with a manual reset pushbutton. An electric static low pressure limit device (LO-STAT) will stop the supply fan whenever fan suction static pressure falls below the 5 WC low limit. The electric static pressure low limit switch will be equipped with a manual reset pushbutton.

3.9.3 Preheat Coil Controll

The preheat coil discharge air temperature (PH-T) of 50°F will be maintained by modulating the preheat coil control valve (PHT-VLV). When the mixed air temperature is above 50°F, the normally open heating valve will be locked out through software interlock. The preheat valve will be closed.

3.9.4 Mixed Air Temperature Control

The discharge air temperature (DA-T) will be maintained by modulating the chilled water control valve (CLG-VLV) in sequence with the mixed air dampers to maintain a setpoint of 55°F as sensed by the discharge air temperature sensor.

3.9.5 Carbon Dioxide Control (Demand Control Ventilation/DCV)

Figure 3.5 shows the Carbon Dioxide control flowchart. Whenever the unit is in the occupied cycle, the outside air minimum will initially be set to operate at 10% of the total fan flow rate. A return air CO_2 sensor, mounted in the common return air ductwork will provide DCV and modulate the outside air damper to limit the CO_2 concentration to 1100ppm. 600ppm above the average outside air concentration of 500ppm, by admitting outside air DCV takes precedence over all other outside air control functions.

3.9.6 Economizer/Mixed Air Damper Control

Anytime the AHU is operating in occupied mode the mixed air damper control will provide minimum outside air, as measured by the outside air flow measuring station (OA-FLOW), or 5% of the fan delivery flow rate. The mixed air dampers will be modulated from minimum position to maximum capacity to provide the economizer operation (45°F< outside air temp <65°F). The mixed air damper will modulate first to maintain discharge air temperature setpoint. Once the mixed air damper is at 100% outside air, mechanical cooling will be enabled to maintain discharge air temperature setpoint. Above the economizer setpoint of 65°F, the mixed air damper will be modulated to control for minimum outside airflow based on DCV while mechanical cooling will maintain the discharge air temperature setponit. DCV will take precedence over all other control operations.

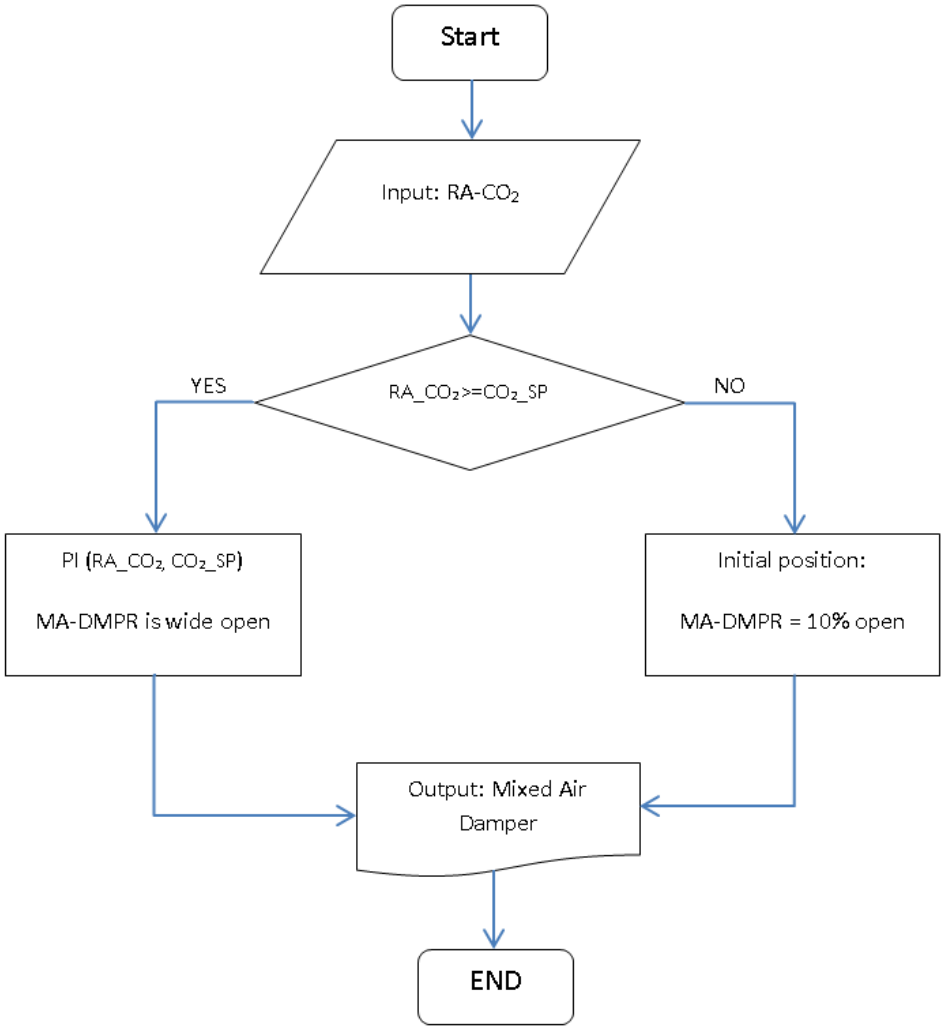

Figure 3.5. Carbon Dioxide Control flowchart

3.9.7 Cooling Coil Control

Cooling coil discharge temperature will be reset from 55°F to 60°F based on the highest zone temperature readings from a range of 70°F to 75°F. Note: we monitor 34 of the 36 zone temperatures to find the highest zone temperature (we exclude the two server room zone temperatures). If either server room zone temperature is above 74°F, we maintain a discharge temperature of 55°F. The discharge air temperature

will be controlled by modulating the normally closed chilled water control valve in sequence with the mixed air dampers per mixed air temperature control, carbon dioxide control and economizer/mixed air damper control.

3.9.8 Heating warm-up (Transition for Unoccupied to Occupied only)

The outside air dampers are to remain closed when the outside air temperature is below 45°F until the return air temperature reaches 68°F. Reheat coil control valves (HTG-VLV) will be modulate to maintain room temperature setpoint. When return air temperature of 68°F is reached, outside air dampers will be placed under automatic control and the system will revert to normal operation.

3.9.9 Cooling Pull-Down (Transition from Unoccupied to Occupied only)

Outside air will be used if outside air temperature is between 45°F and 65°F. Below 45°F, the outside air damper will be closed. Above 65°F the outside air damper will be closed and the cooling coil control valve will modulate to maintain 55°F discharge temperature. When return air temperature drops to 76°F, the system will be placed under automatic control.

3.9.10 Safeties

The unit will be stopped whenever a safety device is tripped. Safety devices will consist of low temperature detection thermostats (low limit), smoke detectors and electric static pressure hi-limit switch (HI-STAT) and electric static pressure low limit switch (LO-STAT).

3.9.11 Cooling Coil Recirculation Pump Control

A cooling coil recirculation pump will be provided to start whenever outside air temperature falls below 40°F. The cooling coil control valve will open to 50% if recirculation loop sensor is less than 40°F in the recirculated loop.

Table 3.2. VAV terminal unit specifications [23]

VAV Boxes	**Model No.**	**Des. CFM**	**Min CFM**	**Max ΔP (WC)**	**Hot Water Coil**			
					MBH	**GPM**	**Rows**	**LAT**
TB-01	DESV-10	1000	600	0.5	29.2	2	2	100
TB-02	DESV-10	1000	600	0.5	29.2	2	2	100
TB-03	DESV-10	1000	600	0.5	13	2	1	75
TB-04	DESV-10	1000	600	0.5	13	2	1	75
TB-05	DESV-10	1000	600	0.5	13	2	1	75
TB-06	DESV-05	300	300	0.5	6.5	1	1	75
TB-07	DESV-07	500	500	0.5	10.9	1	1	75
TB-08	DESV-07	500	500	0.5	10.9	1	1	75
TB-09	DESV-08	700	400	0.5	8.7	1	1	75
TB-10	DESV-07	500	500	0.5	10.9	1	1	75
TB-11	DESV-07	500	500	0.5	10.9	1	1	75
TB-12	DESV-07	500	500	0.5	10.9	1	1	75
TB-13	DESV-09	800	600	0.5	13	2	1	75
TB-14	DESV-09	700	600	0.5	13	2	1	75
TB-15	DESV-07	500	500	0.5	10.9	1	1	75
TB-16	DESV-07	500	500	0.5	10.9	1	1	75
TB-17	DESV-08	600	400	0.5	8.7	1	1	75
TB-18	DESV-08	600	400	0.5	8.7	1	1	75
TB-19	DESV-09	800	600	0.5	13	2	1	75
TB-20	DESV-07	500	500	0.5	10.9	1	1	75
TB-21	DESV-08	750	400	0.5	8.7	1	1	75
TB-22	DESV-08	750	400	0.5	8.7	1	1	75
TB-23	DESV-09	700	700	0.5	34.1	2	2	100
TB-24	DESV-10	925	700	0.5	34.1	2	2	100
TB-25	DESV-05	375	375	0.5	8.1	1	1	75

Table 3.3. AHU I/O list

Type	Parameter		Description	Unit
Analog Inputs	AI1	OA-CFM	Outside Air Flow	CFM
	AI2	MA-T	Mixed Air Temp.	°F
	AI3	SA-CFM	Supply Air Flow	CFM
	AI4	PH-T	Preheat Air Temp.	°F
	AI5	DA-T	Discharge Air Temp.	°F
	AI6	DA-STAT	Discharge Air Static Pressure	In.WC
	AI7	SA-STAT	Supply Air Static Pressure	In.WC
	AI8	CHR-T	Chilled Water Return Temp.	°F
Analog Outputs	AO1	SF-VFD	Supply Fan VFD	-
	AO2	RF-VFD	Return Fan VFD	-
	AO9	MA-DMPR	Mixed Air Damper	%
	AO10	PHT-VALVE	Preheat Valve	%
	*AO11	HUM-OUTPUT	Humidifier Output	
	AO12	CLG-VALVE	Cooling Coil Valve	%
Digital Inputs	DI1	SF-S	Supply Fan Status	-
	DI2	RF-S	Return Fan Status	-
	DI3	CHWP-S	Chilled Water Pump Status	-
	DI4	HILO-STA	HI LO Static Status	-
	DI5	LOWLIMIT	LOWLIMIT Status	-
	DI6	HUM ALARM	Humidity Alarm	-
	DI7	DC ALARM	DC Power Supply Alarm	-
	DI8	TRX-A	Transformer Alarm	-
Digital Outputs	Do3	SF-C	Supply Fan Command	-
	DO4	RF-C	Return Fan Comd	-
	DO5	HUM ENABLE	Humidity Enable	-
	DO6	CHWP-C	Chilled Water Pump Comd	-

Table 3.4. Sensor types installed on the AHU [22]

Sensor Type	**Part NO.**	**Output Signal**	**Range**	**Accuracy**
CHR-T	TE-632AP-1	1k ohm	-50 to 220°F	± 0.73°F at 70°F
RA-T/H	HMD60Y	4-20mA	0-100%RH	± 2% RH
MA-T	TE-6328P-1	1k ohm	-50 to 220°F	± 1.08°F at 70°F
PH-T	TE-6328P-1	1k ohm	-50 to 220°F	± 1.08°F at 70°F
DA-T	TE-6328P-1	1k ohm	-50 to 220°F	± 1.08°F at 70°F
DA-STAT	DPT241	4-20mA	0-10 in WC	± 0.5%

4. MATHEMATICAL MODELING

Sub hourly simulation is essential to predict the energy consumption of an existing AHU and identify the potential energy saving opportunities. The characteristics of all AHU energy consumers should be included in the mathematical model to indicate system performance behaviors and energy consumption patterns.

Five major energy consumption AHU components, including supply fan, return fan, preheat coil, cooling coil and reheat coils, were modeled. Supply fan and return fan consume electricity. Cooling coil uses purchased chilled water while preheat coil and reheat coils utilize purchased hot water.

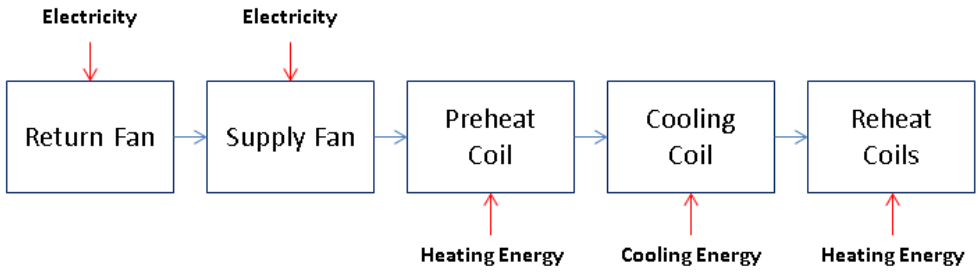

Figure 4.1. Major energy consumers of HVAC system

Chilled water pump and hot water pump were not taken into consideration in the model because the chillers and boilers were not accessible. Humidifiers were not included since they had been abandoned from the system. When supply air is distributed to the terminal units through air ducts, there is heat exchange between the conditioned air and surrounding environment. The heat losses were neglected in the model. Mixed air damper control, cooling coil valve control and preheat coil valve

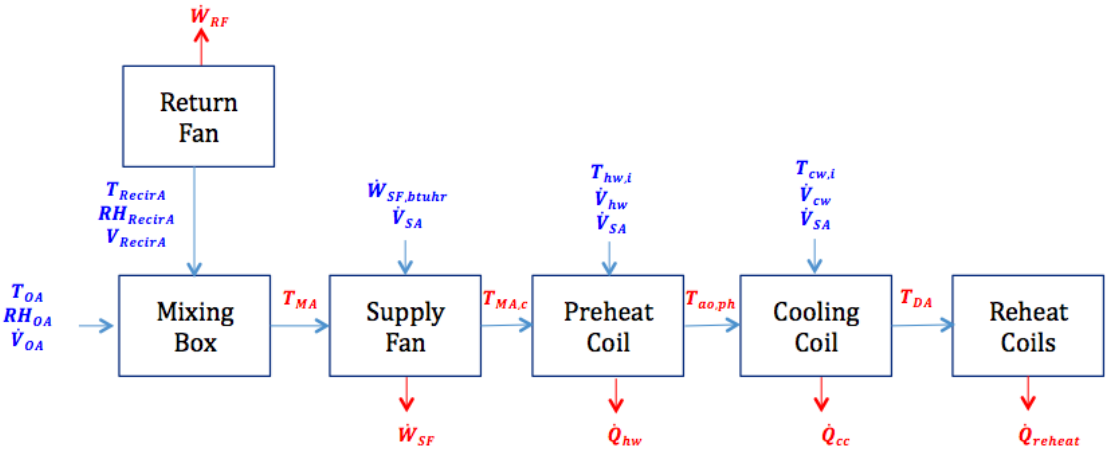

Figure 4.2. Inputs and outputs of the AHU model

control using proportional Integral Derivative (PID) controllers were not developed in the mathematical model due to the scope of the project.

Individual HVAC component was developed as a subprogram in EES. Subprogram could be viewed and modified as a stand-alone program that was able to be called from the main EES program. Subprograms were much more manageable and well-defined compared to a complex integrated program. Once a subprogram was verified and validated, it could be utilized in a wide variety of applications.

The inputs and outputs of the AHU model are shown in Figure 4.2. Most of the inputs for each HVAC component were imported from BAS. Three outside air temperature sensors are installed at different locations on campus to measure the outside dry bulb temperature. The average of the measured three outside air temperatures was utilized by BAS. Outside air relative humidity input was not available in BAS due to the lack of humidity sensor. Thus, the information was gathered from weather.com website for modeling use. The outside air relative humidity collected from weather.com was on an hour-to-hour basis while the sampling interval for BAS was 10 minutes. In order to keep the inputs consistent, the hourly recorded outside

air relative humidity from weather.com was divided into 6 segments with a 10 minutes time window as an input for the mathematical model.

4.1 Mixing Box Model

A portion of return air stream and outside air stream are mixed together in the mixing chamber of the AHU. The mixed air is delivered via draw-through supply fan to be conditioned. As shown in Figure 4.3, the mixing box consists of three sets of dampers: exhaust air damper, outside air damper and return air damper.

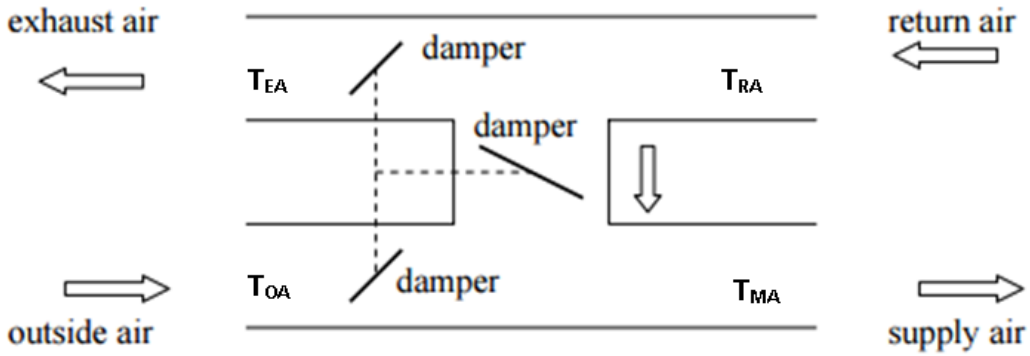

Figure 4.3. Mixing box schematic diagram [27]

Economizer is integrated in the AHU to provide free cooling, or to assist mechanical cooling when the outside condition is appropriate. When the outside air has a lower temperature (or enthalpy) than the supply air set point and cooling is called for, the economizer will be in operation mode by modulating the outside air damper from its minimum position to maximum position. The return air damper is adjusted from its maximum position to minimum position. When the outside air temperature is below or equal to 45°F, the outside air damper is maintained at its minimum position to limit the energy waste to heat up the cold outside air while still

meet indoor air quality requirements. When the outside air temperature is above or equal to 65°F, the outside air damper is adjusted to its minimum position to prevent an increase in cooling load by incorrectly taking in the hot and humid outside air. Exhaust air damper regulates the amount of exhaust air to balance out the static pressure, control moisture and remove contaminants. Flowchart of mixed air damper is shown in Figure 4.4.

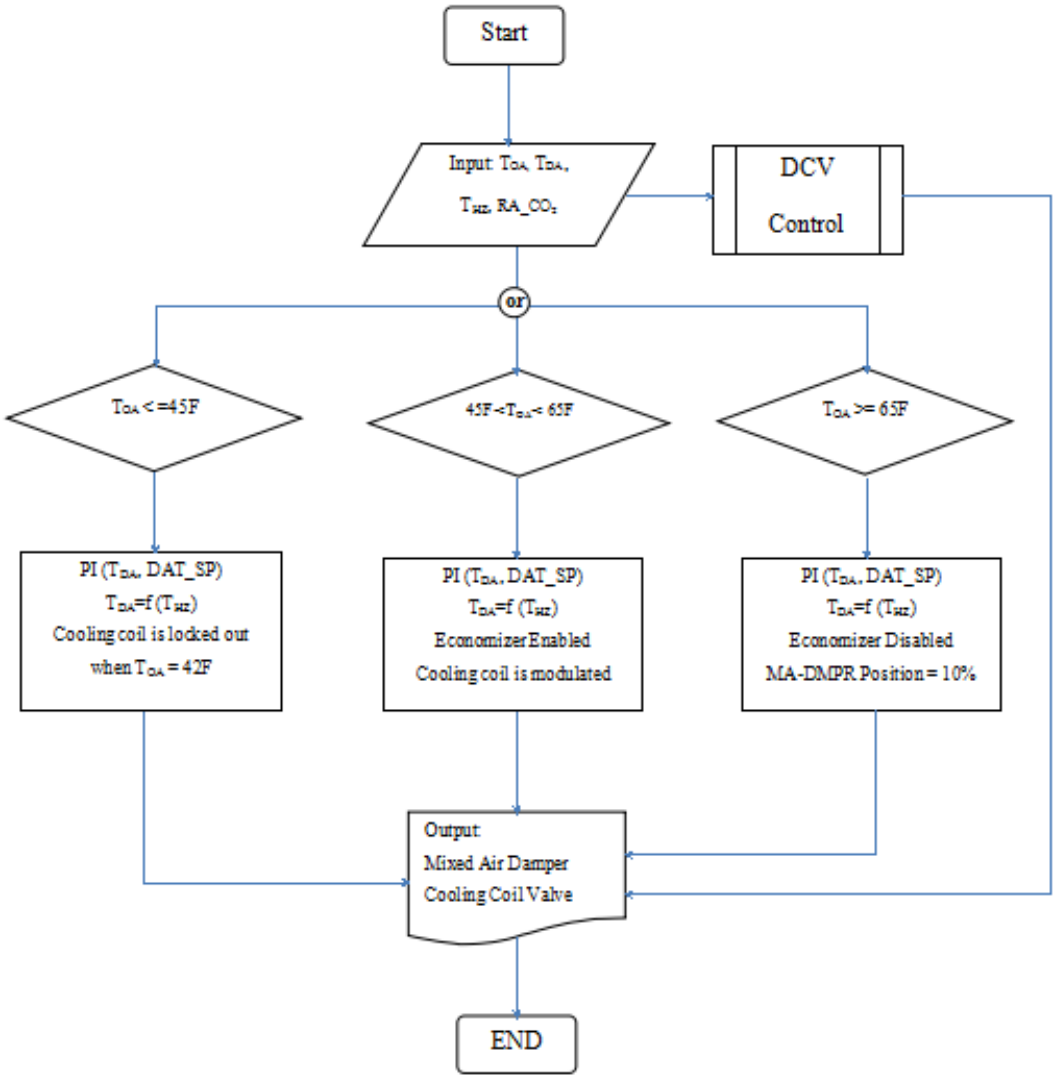

Figure 4.4. Mixing air damper control flowchart

The mass and energy balances can be written as Equation 4.1 and 4.2.

Mass balance equation [14]:

$$\dot{V}_{oa}X_{oa} + \dot{V}_{ra}X_{ra} - \dot{V}_{ea}X_{ea} = \dot{V}_{sa}X_{ma} \tag{4.1}$$

Energy balance equation [28]:

$$\dot{V}_{oa}\rho_{oa}h_{oa} + \dot{V}_{ra}\rho_{ra}h_{ra} - \dot{V}_{ea}\rho_{ea}h_{ea} = \dot{V}_{sa}\rho_{ma}h_{ma} \tag{4.2}$$

The model inputs were from BAS and weather.com website. The output, mixed air temperature, was calculated using the individual model developed in EES.

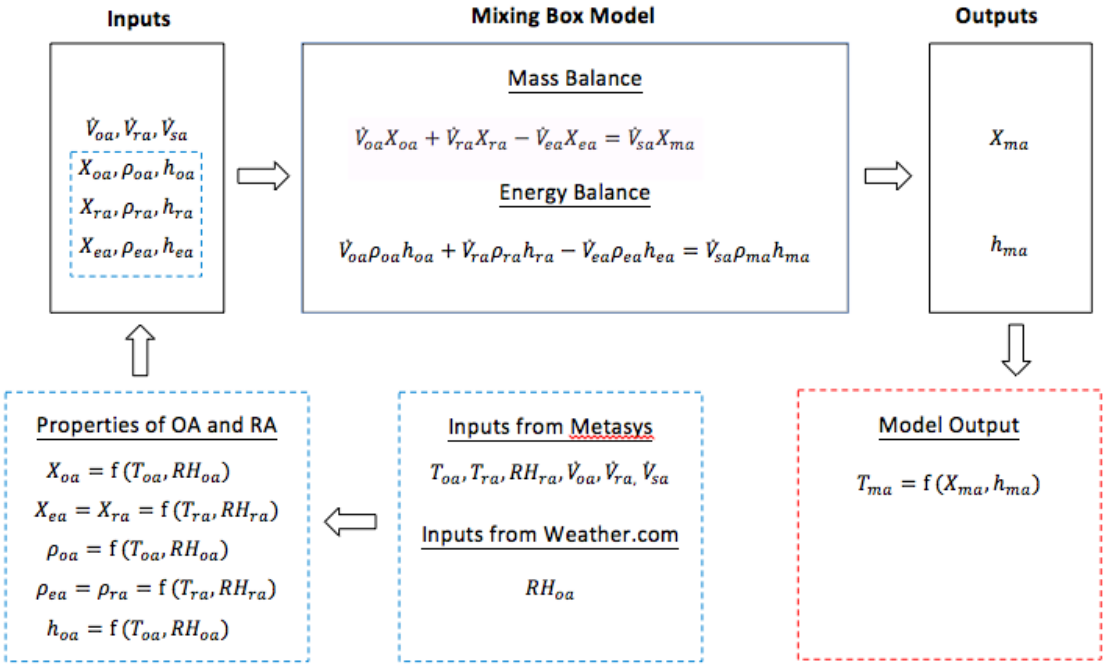

Figure 4.5. Mixing box model logic

4.2 Supply Fan Model

Variable frequency drive (VFD) allows the supply fan motor to run at different speeds to adjust the amount of supply air. pressure sensor is placed at the 2/3 downstream of the main duct to measure the supply air static pressure. VFD is controlled to maintain a constant setpoint of 1.80 in. WC. Supply fan power consumption is a function of static pressure, supply air flow rate and overall efficiency of fan and motor system [14]. Overall efficiency relates to fan shaft efficiency, motor efficiency, efficiency of mechanical transmission, efficiency of control equipment [30].

Supply fan was sized on a design day basis. However, the supply fan runs in part load condition most of time. ASHRAE part load fan model was used to predict the energy use of the supply fan. In Salimifard et al.'s paper [30], a comparison of the actual supply fan power usage to simulated fan power consumption using ASHRAE 90.1 standard part formula and Energy plus formula was made. The paper indicated that the accuracy of the prediction strongly depends on the actual part load curve in specific building. Both part load models were used for the preliminary study. The Equation 4.3 and 4.4 [30] were used for supply fan power calculation because of its high accuracy, comparatively.

$$PLR_{sf} = \frac{\dot{V}_{sa}}{\dot{V}_{sf,design}} \tag{4.3}$$

where PLR_{sf} is part load ratio of supply fan operation (actual CFM/design CFM).

$$\dot{W}_{sf} = (0.0013 + 0.147PLR_{sf} + 0.9506PLR_{sf}^2 - 0.998PLR_{sf}^3) \cdot BHP_{SF} \tag{4.4}$$

where $\dot{W}_{sf}$ is supply fan power and BHP_{SF} is supply fan motor horsepower.

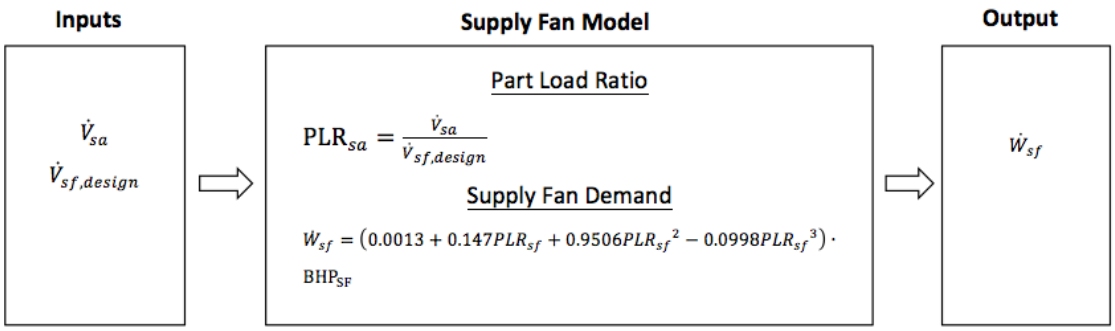

Figure 4.6. Supply fan model logic

4.3 Temperature Rise Across Supply Fan Model

Fan and motor system add heat to the mixed air stream due to fan and motor heat and drive losses. The temperature rise across the supply fan section needs to be considered when calculating the cooling load.

The temperature rise was calculated using the equations from AHU manufacturer product data [31].

$$\dot{W}_{SF,btuhr} = 1.1 \cdot \dot{V}_{SA} \cdot \Delta T_{SF} \tag{4.5}$$

where $\dot{W}_{SF,btuhr}$ is the supply fan motor power output, $\dot{V}_{SA}$ is the supply airflow rate and ΔT_{SF} is the temperature rise across the supply fan section.

4.4 Return Fan Model

The Equation 4.6 and 4.7 [30] were used for return fan power calculation.

$$PLR_{rf} = \frac{\dot{V}_{ra}}{\dot{V}_{rf,design}} \tag{4.6}$$

where PLR_{rf} is part load ratio of return fan operation (actual CFM/design CFM).

$$\dot{W}_{rf} = (0.0013 + 0.147PLR_{rf} + 0.9506PLR_{rf}^2 - 0.998PLR_{rf}^3) \cdot BHP_{RF} \tag{4.7}$$

where $\dot{W}_{rf}$ is return fan power, and BHP_{RF} is return fan motor horsepower.

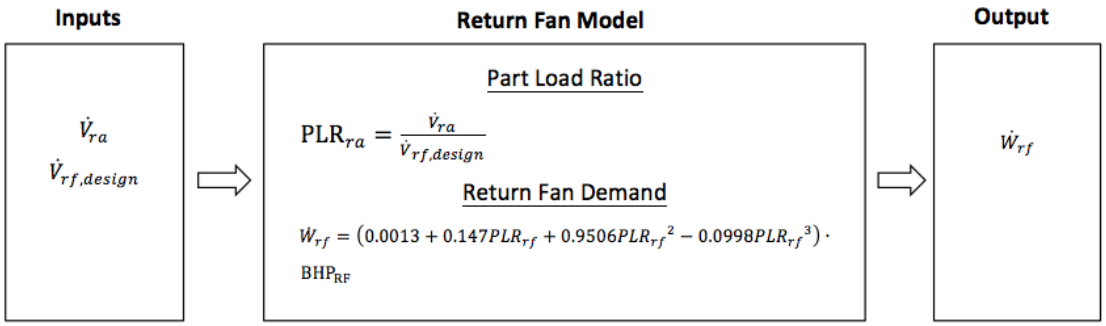

Figure 4.7. Return fan model logic

4.5 Preheat Coil Model

The function of preheat coil is to prevent the cold air freezing the cooling coil. When the mixed air temperature is below 50°F, the preheat coil valve is open to heat up the entering mixed air temperature. The schematic diagram of the preheat coil is displayed in Figure 4.8.

The preheat coil model was based on the model developed by Zajic et al. [32]. In order to simplify the model, a few assumptions have been made.

- The heat transfer between the air and the hot water is in a steady state at a 10 minutes interval. Transient effects are neglected for the air.
- The leaving hot water temperature is assumed to be identical to the mean hot water temperature.
- Latent heat is not taken into consideration. The coil is analyzed as dry coil.
- Constant heat transfer coefficients are used for calculations.

The energy balance on the water side of the coi [32]l:

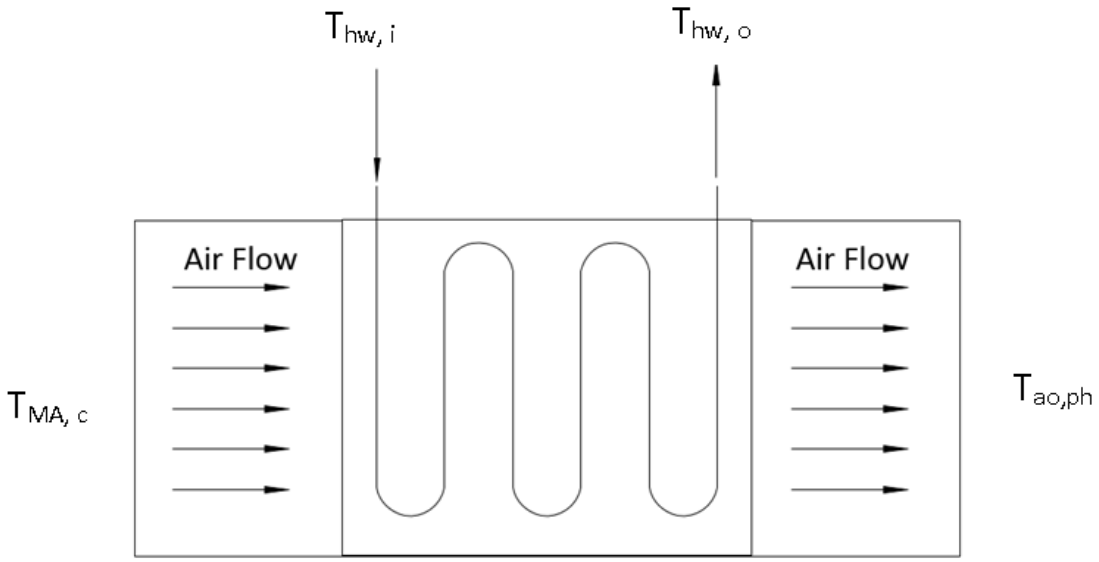

Figure 4.8. Schematic diagram of the pre-heat coil

$$\frac{T_{hw,o}}{t_{interval}} = \frac{1}{c} \cdot [\rho_{hw} \cdot \dot{V}_{hw} \cdot c_{p,hw} \cdot (T_{hw,i} - T_{hw,o}) - \frac{UA_{hw}}{CF_{min,hr}} \cdot (T_{hw,o} - T_{ao,ph})] \quad (4.8)$$

The energy balance on the air side of the coil [32]:

$$\frac{T_{ao,ph}}{t_{interval}} = \frac{1}{c_{p,ma,c}} \cdot [\frac{UA_{hw}}{CF_{min,hr}} \cdot (T_{hw,o} - T_{ao,ph}) - \rho_{ma,c} \cdot \dot{V}_{SA} \cdot c_{p,ma,c} \cdot (T_{ao,ph} - T_{ma,c})] \quad (4.9)$$

Inputs: $\dot{V}_{hw}$, $\dot{V}_{sa}$, $T_{hw,i}$, $T_{MA,c}$

Outputs: $T_{ao,ph}$, $T_{hw,o}$

Parameters: c, UA_{hw}, $t_{interval}$, $CF_{min,hr}$

c is the overall thermal capacity, UA_{hw} is the overall heat transfer coefficient, $t_{interval}$ is the sampling interval and $CF_{min,hr}$ is the conversation factor (converting minutes to hour).c is estimated as 0.09 $Btu/°F$. The heat transfer surface of the preheat coil is 40 square feet. Overall heat transfer coefficient per square feet is

estimated as 50 $Btu/hr\text{-}ft^2\text{-}^\circ F$ [33]. Thus, the overall heat transfer coefficient is 1000 $Btu/hr\text{-}^\circ F$.

Theoretically, valve water flow is a function of pressure drop across the loop including the valve and coil, valve open position, the inherent valve characteristics, flow coefficients and valve authority [34, 35]. The valve open position could be read from BAS. However, differential pressure across the coil and valve was unknown. Installed valve characteristics were infeasible to estimate without manufacturer data. Therefore, a linear relationship between the valve open position and water flow rate was adopted in the mathematical model.

Preheat coil energy consumption at 10 minutes interval:

$$Q_{hw} = \rho_{ma,c} \cdot \dot{V}_{SA} \cdot c_{p,ma,c} \cdot (T_{ao,ph} - T_{ma,c}) \cdot t_{interval} \tag{4.10}$$

4.6 Cooling Coil Model

Figure 4.9 shows the schematic diagram of the cooling coil. The supply air temperature was set at 55°F. When is greater than supply air temperature setpoint, the cooling coil valve is modulated to cool down supply air temperature to its setpoint.

The cooling coil model is also based on the model developed by Zajic et al. [32]. The assumptions for preheat coil model apply to cooling coil model as well.

The energy balance on the water side of the coi [32]l:

$$\frac{T_{cw,o}}{t_{interval}} = \frac{1}{c} \cdot [\rho_{cw} \cdot \dot{V}_{cw} \cdot c_{p,cw} \cdot (T_{cw,i} - T_{cw,o}) - \frac{UA_{cc}}{CF_{min,hr}} \cdot (T_{cw,o} - T_{a,o})] \tag{4.11}$$

The energy balance on the air side of the coil [32]:

$$\frac{T_{a,o}}{t_{interval}} = \frac{1}{c_{p,ma,c}} \cdot [\frac{UA_{cc}}{CF_{min,hr}} \cdot (T_{cw,o} - T_{a,o}) - \rho_{ma,c} \cdot \dot{V}_{SA} \cdot c_{p,ma,c} \cdot (T_{a,o} - T_{a,i})] \tag{4.12}$$

Inputs: $\dot{V}_{cw}$, $\dot{V}_{SA}$, $T_{cw,i}$, $T_{a,i}$

Outputs: $T_{a,o}$, $T_{cw,o}$

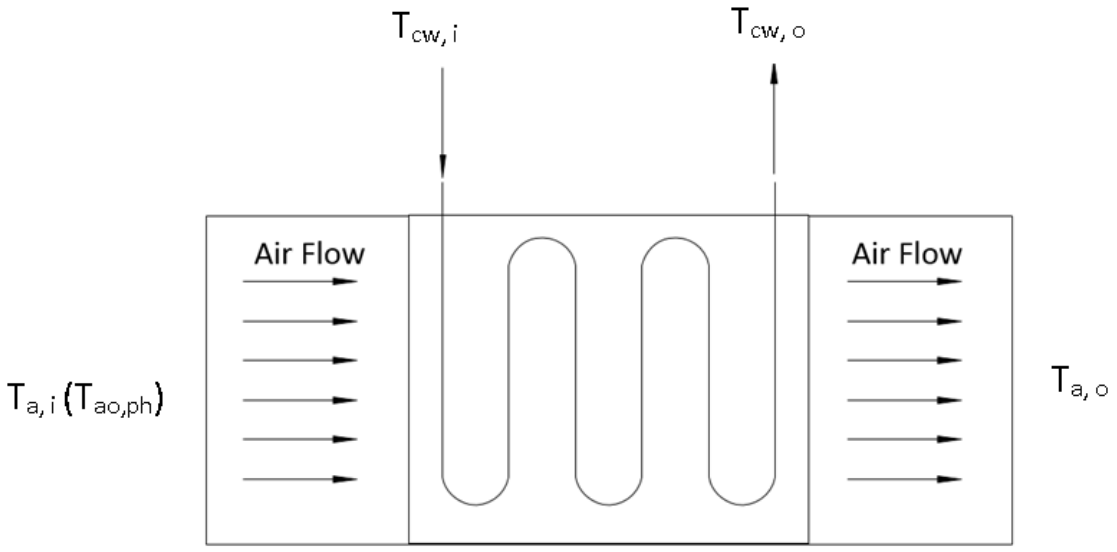

Figure 4.9. Schematic diagram of the cooing coil

Parameters: c, UA_{cc}, $t_{interval}$, $CF_{min,hr}$

The heat transfer surface of the preheat coil is 40 square feet. Overall heat transfer coefficient per square feet is estimated as 15 $Btu/hr\text{-}ft^2\text{-}^\circ F$ [33]. Thus, the overall heat transfer coefficient is 600 $Btu/hr\text{-}^\circ F$.

Cooling energy consumption is a function of supply air flow rate, supply air density and temperature difference between supply air and discharge air.

Cooling coil energy consumption at 10 minutes interval:

$$Q_{cc} = \rho_{ao,ph} \cdot \dot{V}_{SA} \cdot c_{ao,ph} \cdot (T_{ao,ph} - T_{DA}) \cdot t_{interval} \tag{4.13}$$

where T_{DA} is discharge air temperature, which is the same as $T_{a,i}$.

4.7 Zone Model

VAV system controls the zone temperature by modulating the airflow while maintaining the constant supply air temperature setpoint. The targeted AHU serves 36

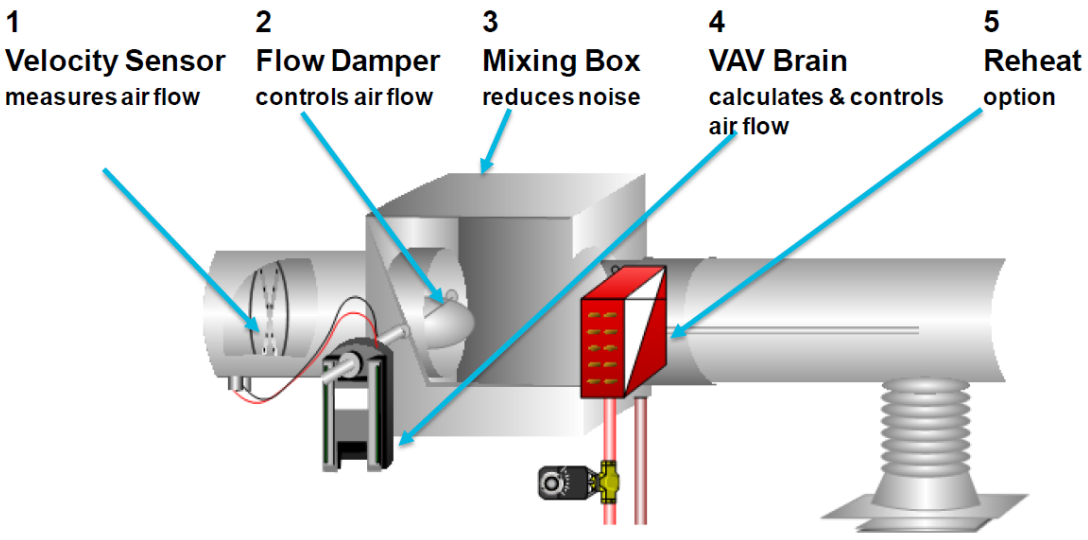

Figure 4.10. Components of a VAV box [36]

VAV terminal boxes throughout the ET basement. The damper position of the individual terminal unit varies to meet the desired room temperature. Reheat coil is included in the VAV box to heat the entering supply air in order to meet the local zone temperature setpoint. The components of a VAV box are shown in Figure 4.10.

In order to simplify the calculations, 36 VAV boxes were considered as a single VAV box.

Reheat coilsl energy consumption at 10 minutes interval:

$$Q_{rh} = \rho_{DA} \cdot \dot{V}_{SA} \cdot (h_{RA} - h_{DA}) \cdot t_{interval} \tag{4.14}$$

5. RESULTS AND VALIDATIONS

5.1 AHU Model Validation

Long trends on DA-T, RA-T, RA-H, SA-STAT, OA-CFM, SA-CFM, RA-CFM, MA-T, PH-T, PHT-VLV, CLG-VLV, OA-T, SF POWER , and RF POWER were collected from February 1 to February 28 and from March 1 to March 31 as inputs for the mathematical model. The details of data set are shown in Table 5.1.

Table 5.1. Description of data sets for model validation

Data Set No.	**Time Period**	**Sampling Time**	**Number of Samples**	**Average OA-T**
1	2/1/2015-2/28/2015	28 days	4032	20°F
2	3/1/2015-3/31/2015	22 days	3146	40°F

The cooling valve was shut down from March 10 to March 15 for replacement. The days were excluded in the Data set 2 due to AHU abnormal operation.

When the first data set was collected, the discharge air temperature was set as 55°F while the supply air static pressure setpoint was 1.80 in.WC.

The output of each component was calculated and then compared with measured data.

5.1.1 Mixing Box Model Validation

Figure 5.1 demonstrates that the simulated mixed air temperature trend followed a similar pattern as the real time trend. However, errors existed between the simulated and measured mixed air temperature.

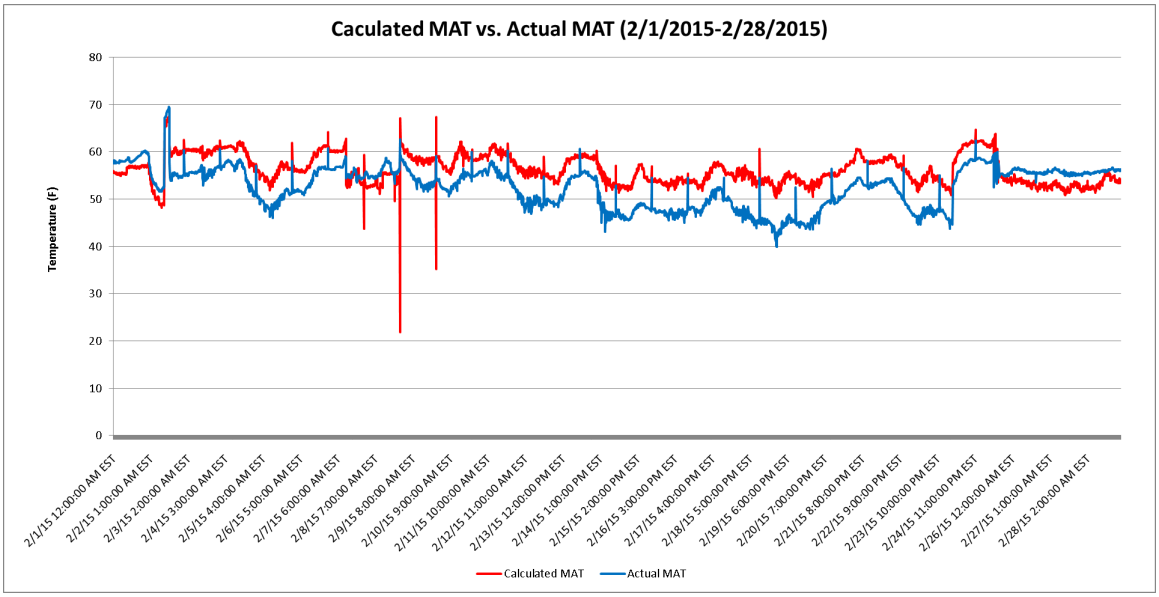

Figure 5.1. Calculated MA-T vs. Actual MA-T (2/1/2015-2/28/2015)

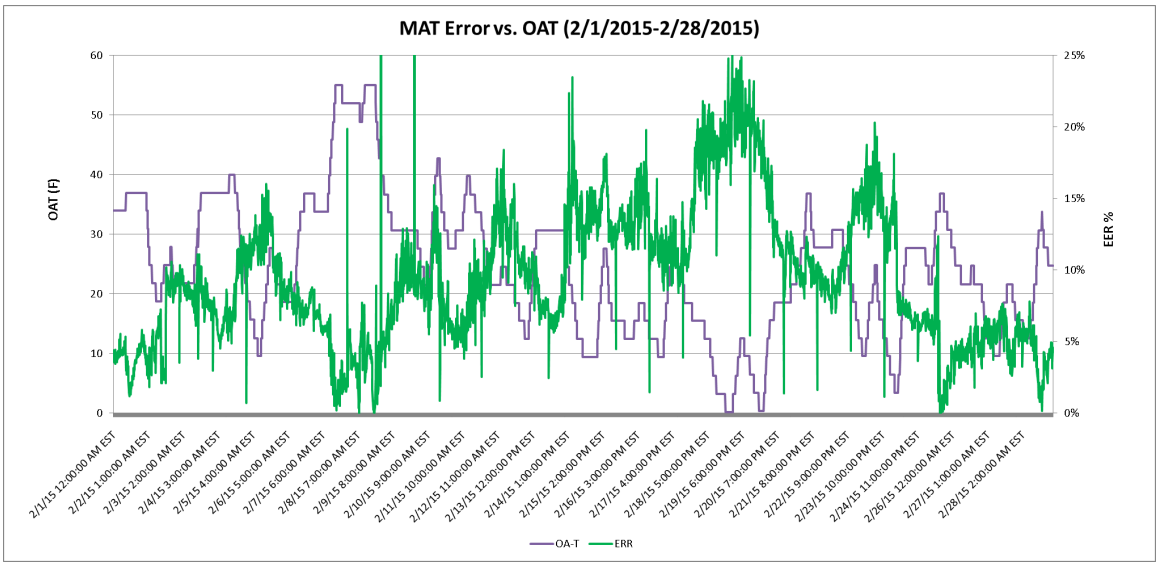

Figure 5.2. MA-T Error vs. OAT (2/1/2015-2/28/2015)

Figure 5.2. shows that the error between the measured MA-T and predicted MA-T varies with the outdoor air temperature. When the outdoor air temperature was

low, the predicted MA-T tended to be less accurate. The error could be caused by the fact that OAT sensor was not calibrated, or this type of temperature sensor was less precise when operating in lower ambient temperature condition.

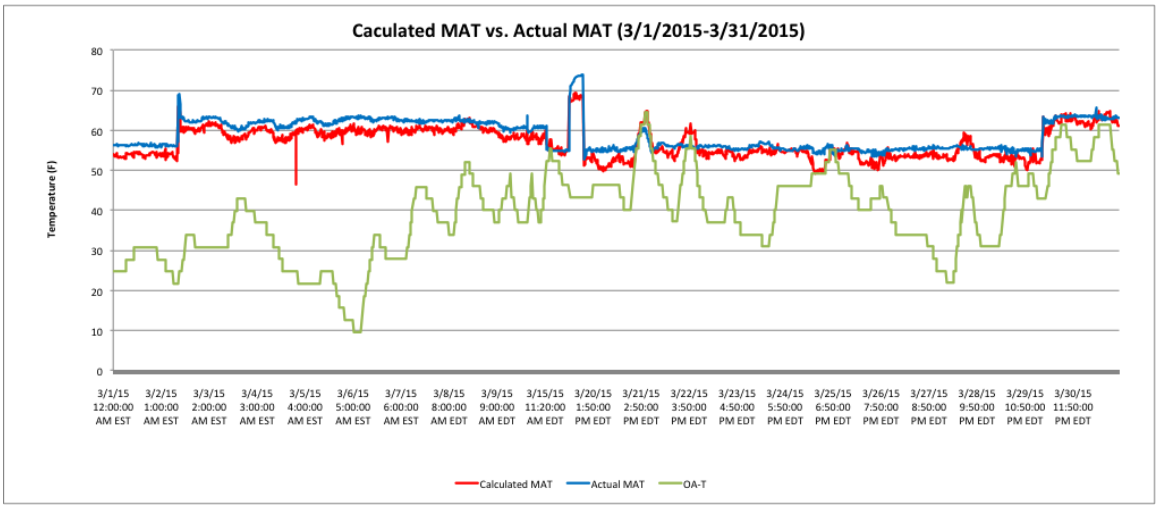

Figure 5.3. Calculated MA-T vs. Actual MA-T (3/1/2015-3/31/2015)

Figure 5.3 shows the calculated and actual mixed air temperature from March 1 to March 31. In general, calculated MA-T was slightly lower than actual MA-T.

5.1.2 Supply Fan Model Validation

As shown in Figure 5.4, simulated supply fan power was off measured supply fan power. According to Salimifard et al. [30], the simulation performance heavily depends on how the fan is setup in a specific building. The error percentage of supply fan power will be lower by applying the actual part load fan curve.

Figure 5.5 describes the correlation between real time supply fan power and predicted supply fan power. R-squared value interprets how well the model fits the data. The higher the R-squared value, the less variance is between real data and predicted data [37].

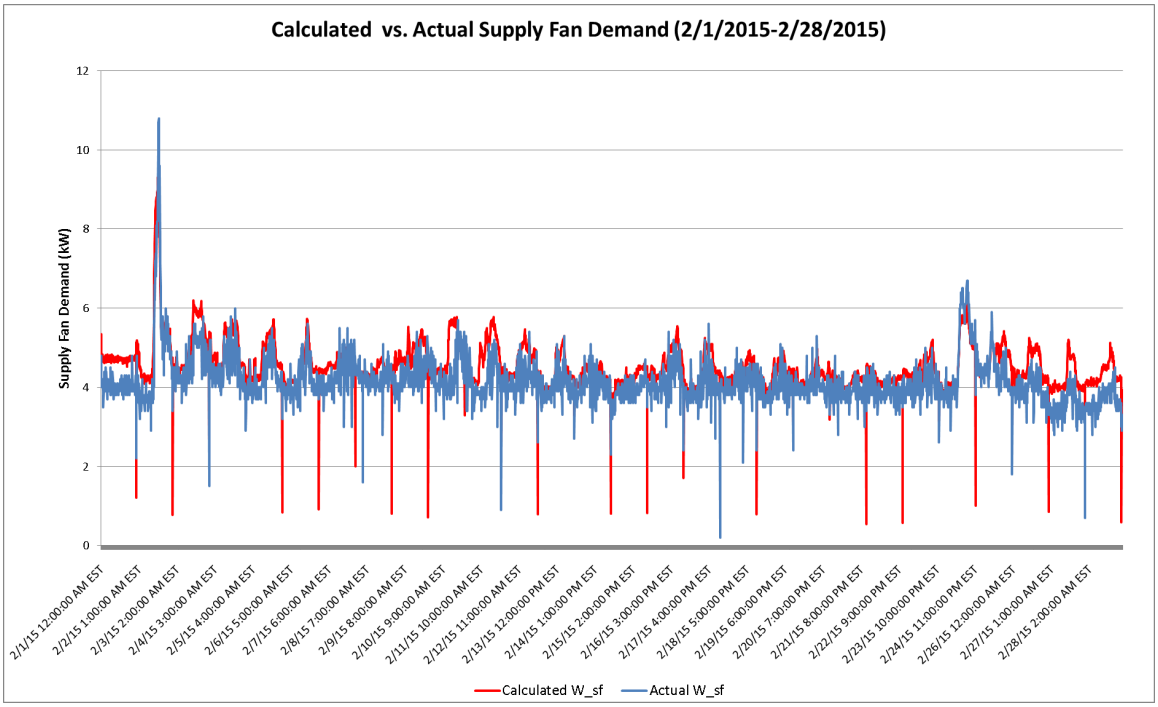

Figure 5.4. Calculated supply fan power vs. measured supply fan power (2/1/2015-2/28/2015)

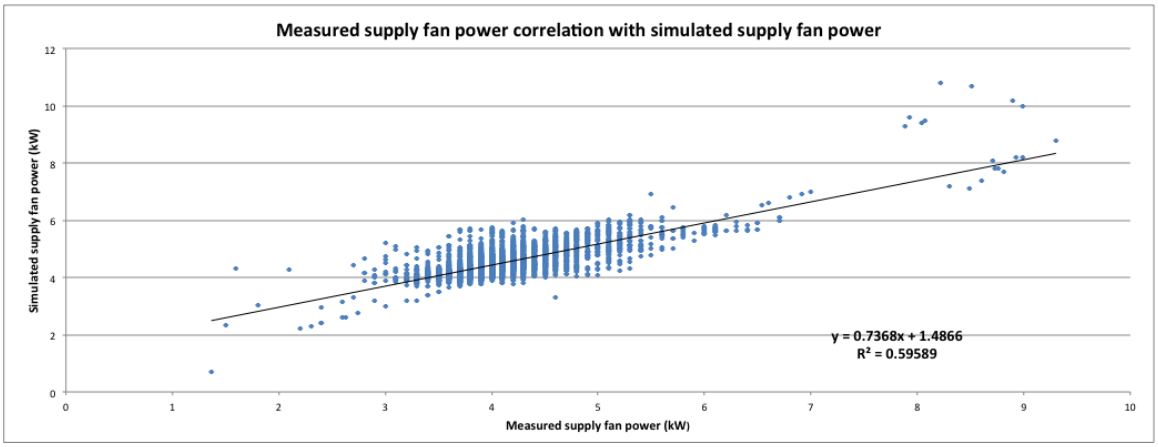

Figure 5.5. Correlation between measured supply fan power and predicted supply fan power

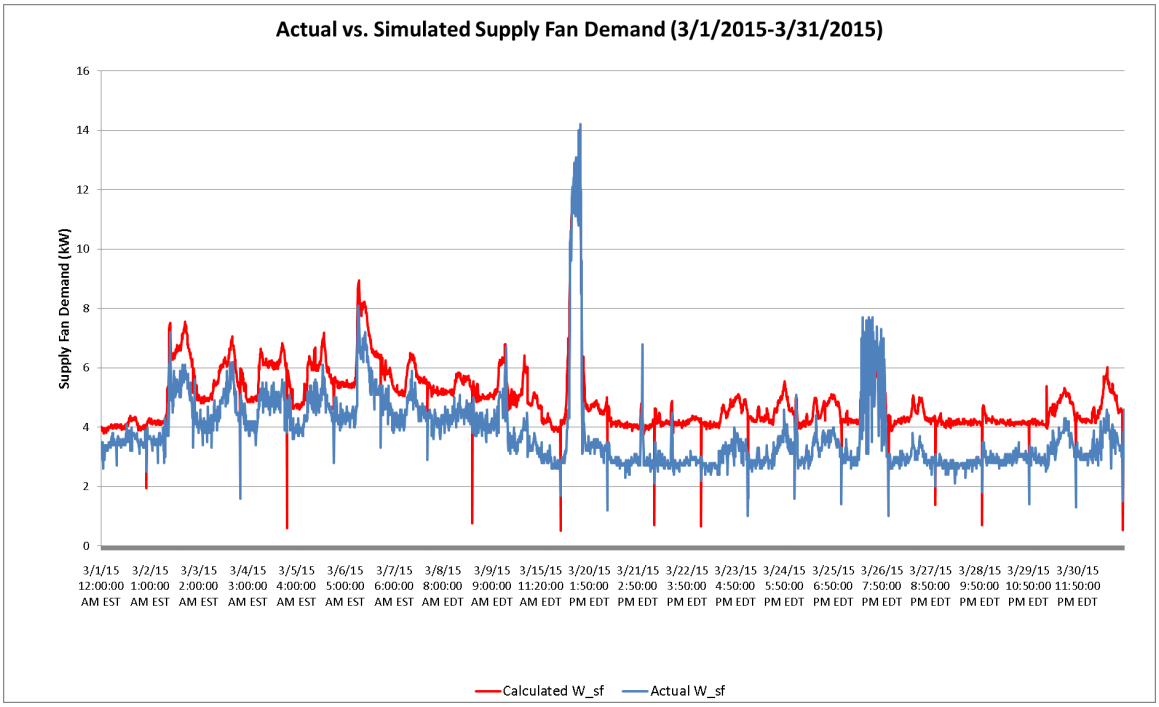

Figure 5.6. Calculated supply fan power vs. measured supply fan power (3/1/2015-3/31/2015)

Figure 5.6 presents that error different between calculated supply fan power and actual supply fan power from March 1 to March 31 was much higher than from February 1 to February 28.

5.1.3 Return Fan Model Validation

The RA fan was being kept at a minimum speed in order to keep the mixed air damper at its minimum position. It allows minimum OA flow to maintain the required DA-T. Figure 5.7 and Figure 5.8 indicate that error percentage was really high when applied ASHRAE part load fan power equation to return fan. The return fan model needed to be calibrated in order to better predict the fan power.

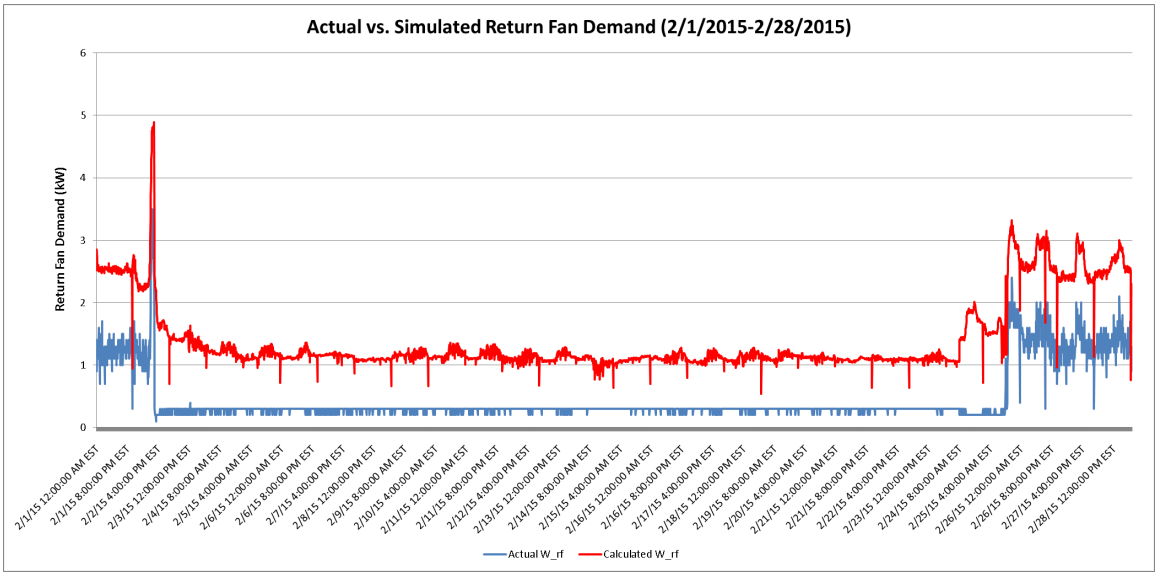

Figure 5.7. Actual vs. Simulated return fan power (2/1/2015-2/28/2015)

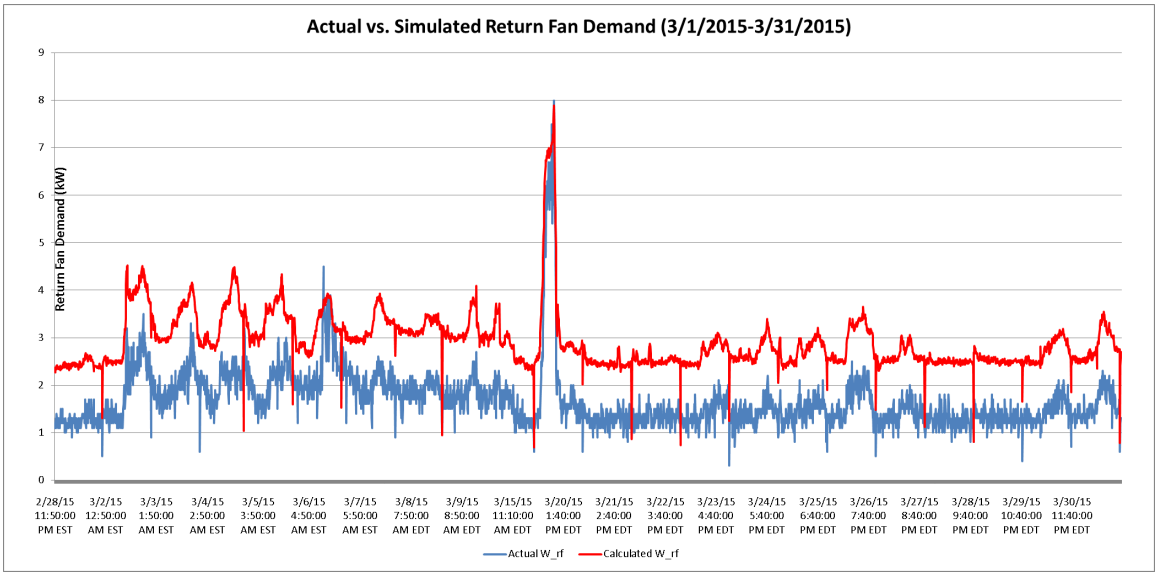

Figure 5.8. Actual vs. Simulated return fan power (3/1/2015-3/31/2015)

Figure 5.9 showed the correlation between the actual return fan power and simulated return fan power using ASHRAE part load fan power equation. The calibrated return fan power can be expressed as Equation 5.1.

$$CalibratedW_rf = (CaculatedW_rf - 0.9417)/1.1329 \tag{5.1}$$

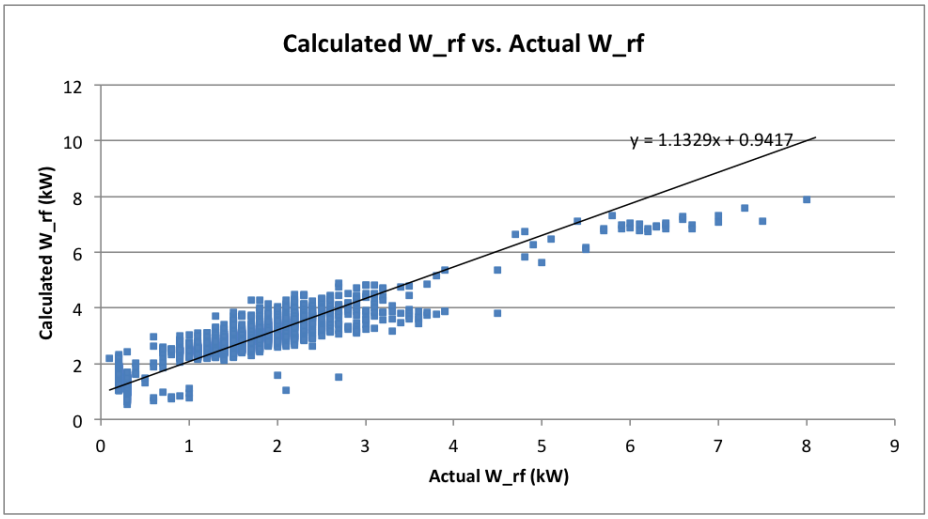

Figure 5.9. Correlations between calculated and actual return fan power

Figure 5.10 and Figure 5.11 show the error between actual return fan power and predicted return fan power after calibration.

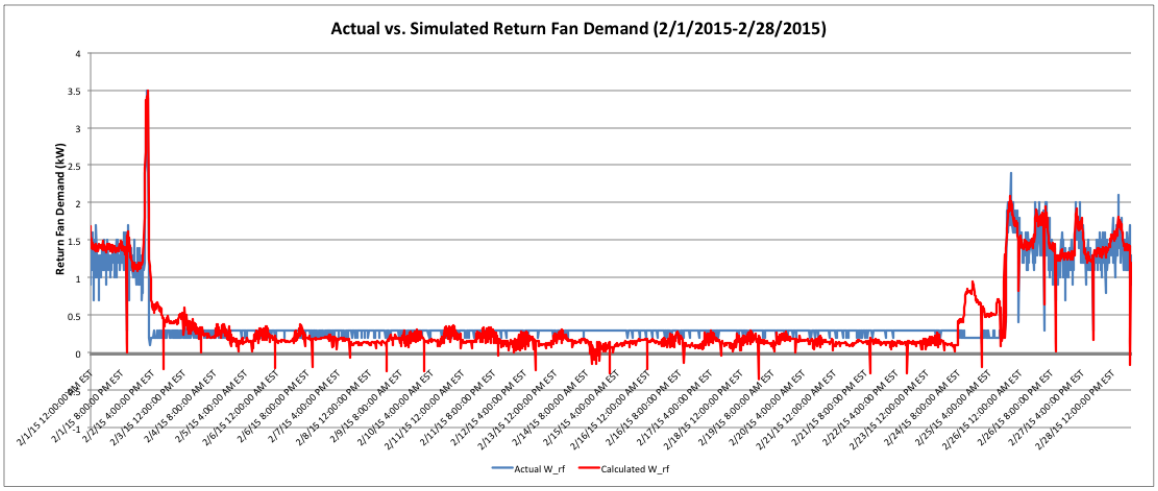

Figure 5.10. Actual return fan power vs. Simulated return fan power after calibration (2/1/2015-2/28/2015)

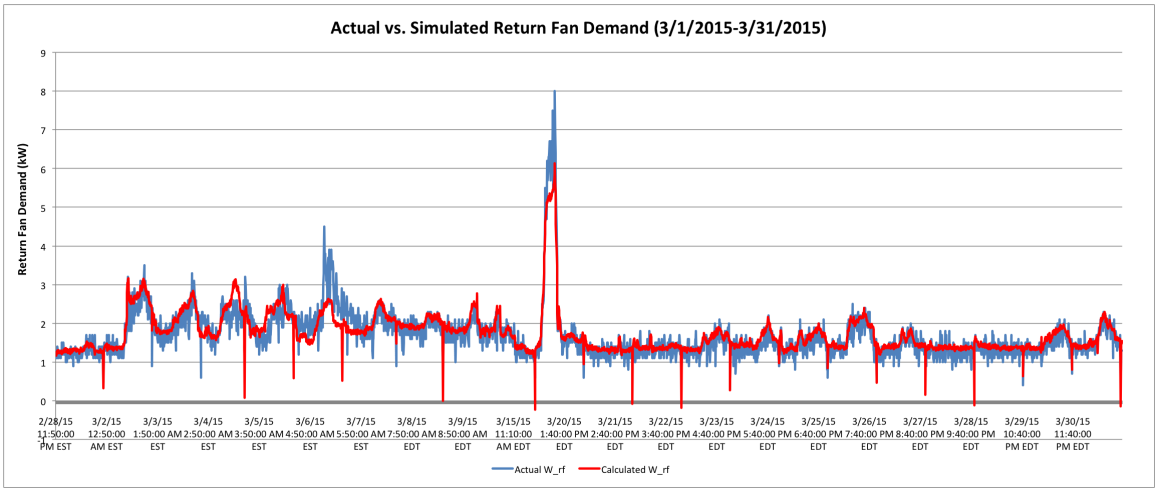

Figure 5.11. Actual return fan power vs. Simulated return fan power after calibration (3/1/2015-3/31/2015)

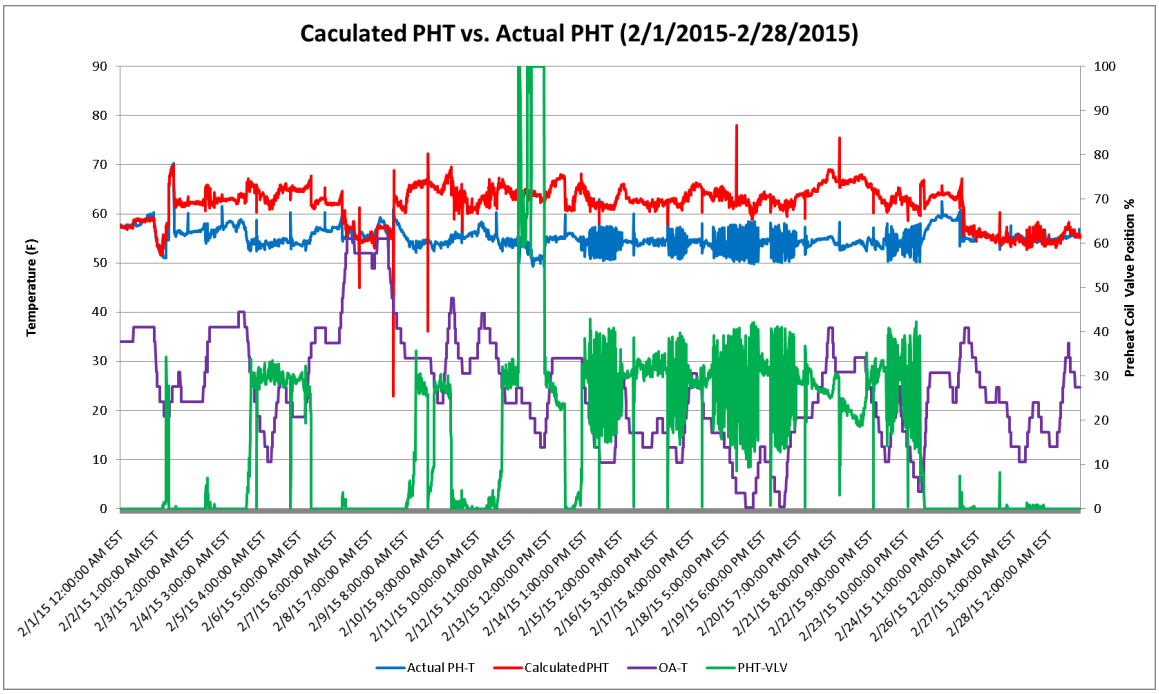

Figure 5.12. Calculated PH-T vs. Actual PH-T (2/1/2015-2/28/2015)

5.1.4 Preheat Coil Model Validation

The green line in Figure 5.12 presents the open percentage of the preheat coil valve. The simulated PH-T was generally higher than the actual PH-T. Since MA-T was an input for PH-T calculation, the error between the measured PH-T and calculated PH-T might partly result from the uncertainty of MA-T. From February 1 to February 2, February 7 to February 9, and February 24 to February 28, the error between predicted PH-T and actual PH-T was low.

As displayed in Figure 5.13, calculated and simulated preheat coil leaving air temperatures were very close. The preheat coil valve was 100% closed during the majority of time from March 1 and March 31, which means there was no heat transfer between hot water and air. So the preheat coil leaving air temperature was equal to the mixed air temperature plus temperature rise across the supply fan.

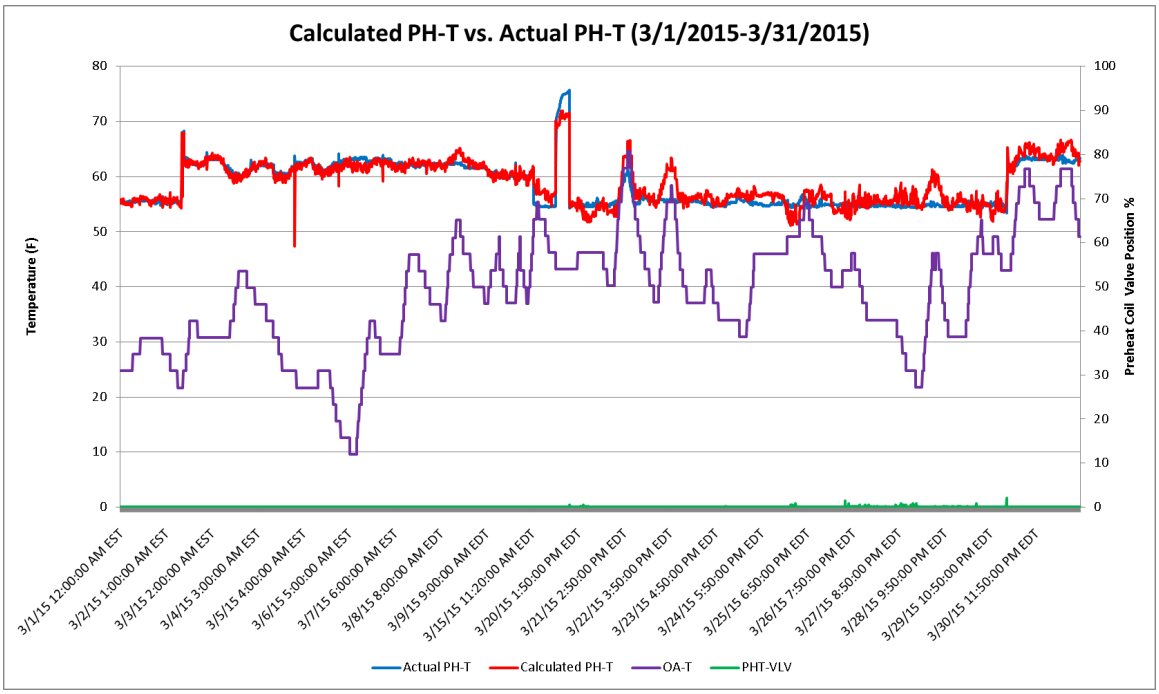

Figure 5.13. Calculated PH-T vs. Actual PH-T (3/1/2015-3/31/2015)

5.1.5 Cooling Coil Model Validation

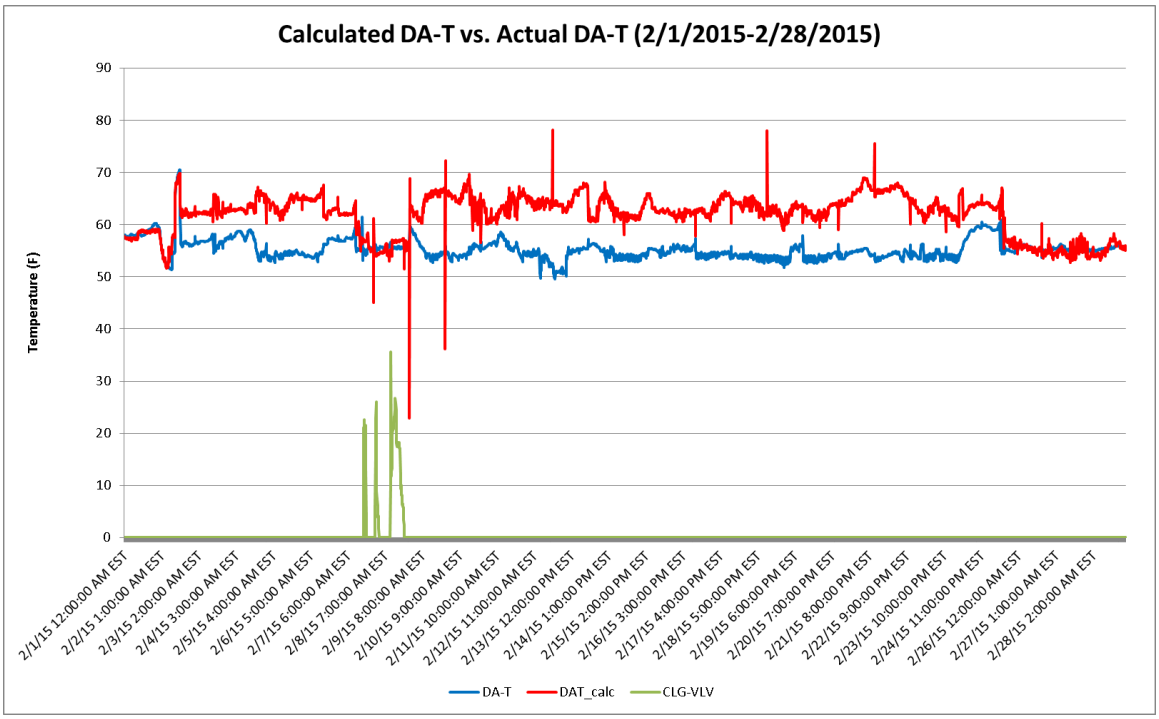

Figure 5.14. Calculated DA-T vs. Actual DA-T (2/1/2015-2/28/2015)

From Figure 5.14 we can see that the cooling coil valve was open from February 7 to February 9. During this period, calculated discharge air temperature and actual discharge air temperature was close. The error between simulated DA-T and actual DA-T was relatively high most of time in February due to the MA-T error in mixed air box model as input. According to Figure 5.15, the DA-T prediction was more accurate from March 1 to March 31.

5.2 Error Rate Analysis

Mean Absolute Percentage Error (MAPE) and Root Mean Square Deviation (RMSD) have been employed to measure the accuracy of the mathematical model.

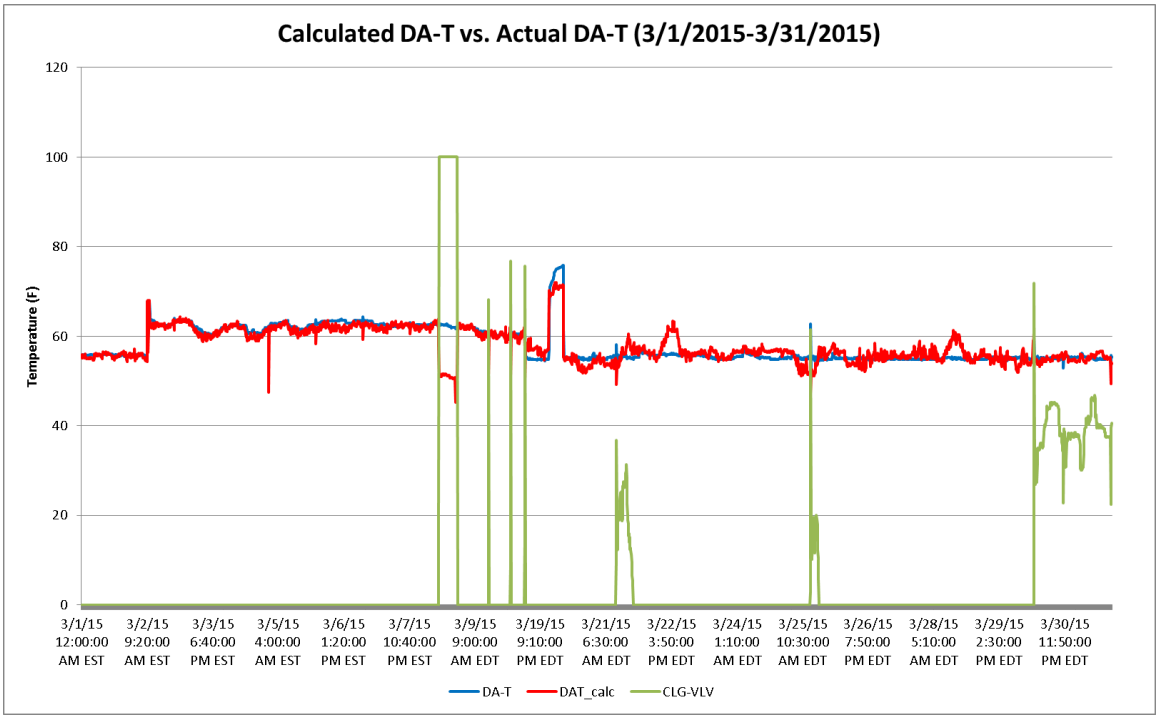

Figure 5.15. Calculated DA-T vs. Actual DA-T (3/1/2015-3/31/2015)

Both MAPE and RMSD are widely used to measure the average magnitude of the errors.The definitions of MAPE and RMSD are shown in Equation 5.2 [38] and Equation 5.3 [39].

$$MAPE = \frac{100\%}{n} \sum_{t=1}^{n} |\frac{y - \hat{y}_t}{y}| \tag{5.2}$$

$$RMSD = \sqrt{\frac{\sum_{t=1}^{n} (\hat{y}_t - y)^2}{n}} \tag{5.3}$$

where y is the actual value, $\hat{y}$ is the predicted value, t is the sampling time and n is the number of sample points.

Table 5.2 displays the error differences comparison for each component model using different data sets. Generally speaking, model prediction using the second data

set was more accurate except supply fan model. The outdoor air temperature was higher from March 1 to March 31, which might contribute to the level of accuracy.

Table 5.2. Error differences comparison for individual model

Parameter	**2/1/2015-2/28/2015 Avg. OAT 20 °F**		**3/1/2015-3/31/2015 Avg. OAT 40 °F**	
	MAPE	**RMSD**	**MAPE**	**RMSD**
MA-T	6.85%	5.27	3.61%	2.4
W_SF	11.99%	0.58	34.63%	1.25
W_RF	49.39%	0.19	12.76%	0.3
PH-T	12.95%	8.22	2.01%	1.66
DA-T	12.66%	8.03	2.23%	2.22

5.3 Baseline Energy Consumption

Energy consumption of each element was calculated using the first data set from February 25 to February 28. All the individual components were integrated to calculate the overall energy consumption. The overall energy consumption was the baseline model without using any reset control strategies. The details are shown in Table 5.3. The baseline energy consumption was used for comparison in Chapter 7.

Table 5.3. Baseline energy consumption

Q_rh (BTU)	9633080
Q_cc (BTU)	0
Q_hw (BTU)	130893
E_SF (BTU)	1242296
E_RF (BTU)	420964
Q_total (BTU)	9633080

6. UNCERTAINTY ANALYSIS

The inputs to the mathematical model are measured data with some uncertainty, which cause the uncertainty of the calculated outputs. Uncertainty propagation is a process that tracks how the uncertainty of the measured parameters results in the uncertainty in output variables [20, 40].

The purpose of the uncertainty analysis is to identify the influence of individual input variable on the predicted outputs of the simulation model. Uncertainly analysis was implemented in EES using the Root Sum Square (RSS) method to rank the order of the independent variables with respect to the impact on the outputs of the model [40].

The theoretical background of the uncertainty propagtion is excertped from Mastering EES manual [40]. If the calculated quantity (Q) is a function of N measurements (x_1 through x_N) each with its own uncertainty (u_{x_1} through u_{x_N}):

$$Q = Q(x_1, x_2, ..., x_N) \tag{6.1}$$

Then the uncertainty in $Q(u_Q)$ can be divided into its elementary uncertainties due to each of the measured variables (u_{Q,x_1} through u_{Q,x_N}). The elementary uncertainty in Q due to measurement is given by x_i:

$$u_{Q,x_i} = \frac{\partial Q}{\partial x_i} u_{x_i} \tag{6.2}$$

The elementary uncertainties can be combined to provide the total uncertainty in Q by taking the square root of the sum of squares of the elemental uncertainties:

$$u_Q = \sqrt{u_{Q,x_1}^2 + u_{Q,x_2}^2 + ... + u_{Q,x_N}^2} \tag{6.3}$$

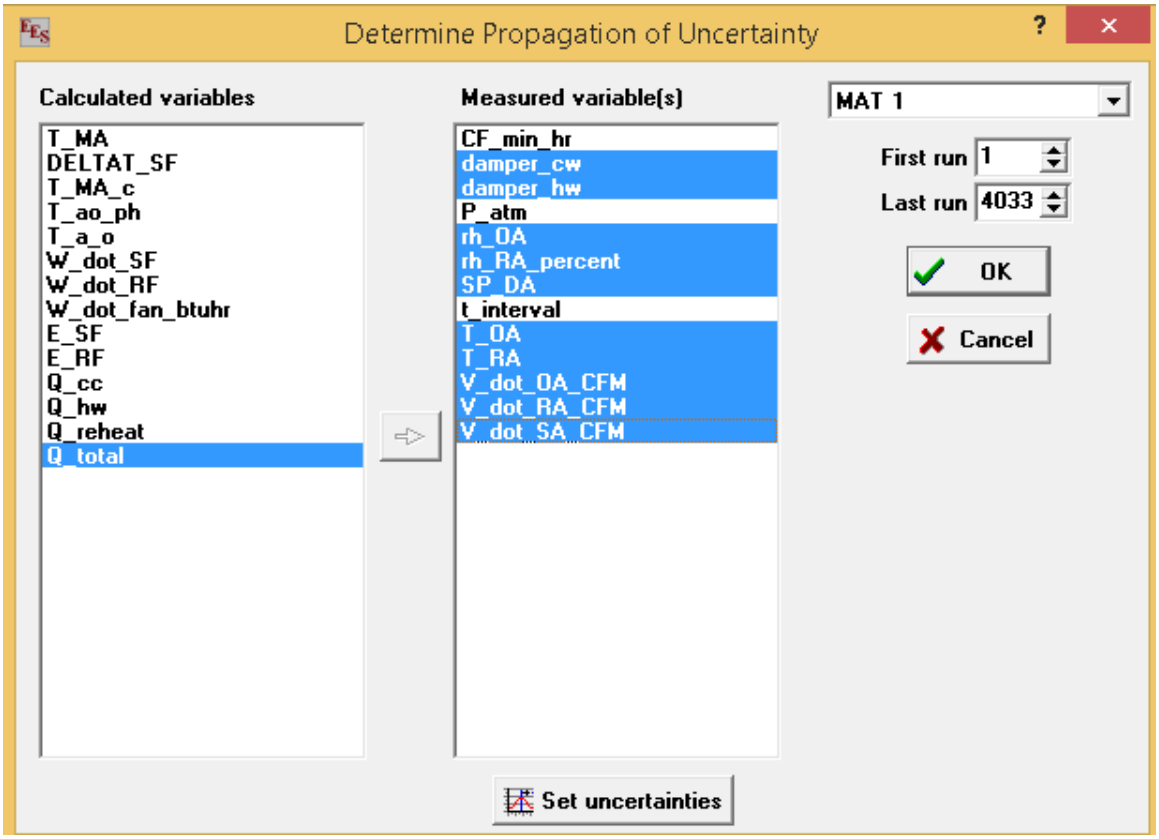

Figure 6.1. Uncertainty propagation

Uncertainty propagation is carried out automatically using the RSS method in EES program. Uncertainty values of measured variables can be specified to determine the overall uncertainty in calculated variables [40].

As shown in Figure 6.1, measured variables are cooling coil valve position, preheat coil valve position, outdoor air temperature, return air temperature, outdoor air humidity, return air humidity, outdoor air flow rate, return air flow rate, supply air flow rate and supply air static pressure. The calculated variable is the total energy consumption, which consists of electricity usage from supply fan and return fan, cooling energy consumption from cooling coil and heating energy consumption from heating coil and reheat coils in VAV terminal units.

Uncertainty values are assigned to measured variables in Figure 6.2.

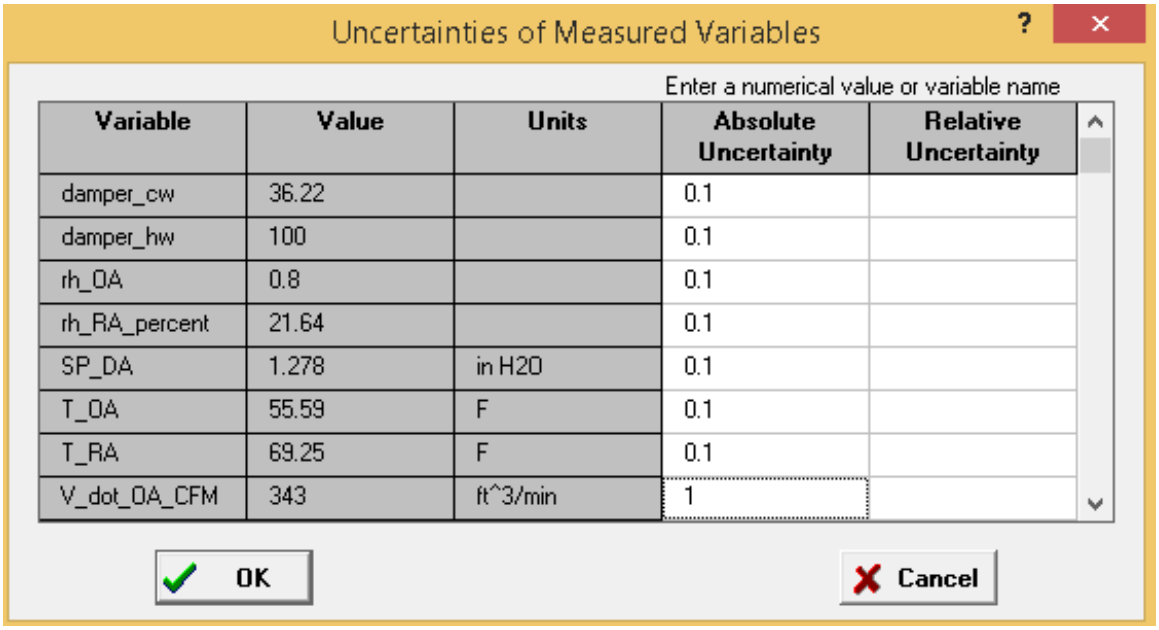

Figure 6.2. Uncertainties of measured variables

Unit Settings: Eng F psia mass deg

(MAT, Run 4033)

Variable±Uncertainty	**Partial derivative**	**% of uncertainty**
Q_{total} = 20420±122.6 [Btu]		
$damper_{cw}$ = 0±0.1	$\partial Q_{total} / \partial\, damper_{cw}$ = 0	0.00 %
$damper_{hw}$ = 100±0.1	$\partial Q_{total} / \partial\, damper_{hw}$ = 201.5	2.70 %
SP_{DA} = 1.647±0.1 [in H2O]	$\partial Q_{total} / \partial\, SP_{DA}$ = 0	0.00 %
T_{OA} = 24.72±0.1 [F]	$\partial Q_{total} / \partial\, T_{OA}$ = -644	27.62 %
T_{RA} = 68.88±0.1 [F]	$\partial Q_{total} / \partial\, T_{RA}$ = 558	20.73 %
$\dot{V}_{OA,CFM}$ = 222.8±1 [ft^3/min]	$\partial Q_{total} / \partial\, \dot{V}_{OA,CFM}$ = 85.68	48.88 %
$\dot{V}_{RA,CFM}$ = 673.5±1 [ft^3/min]	$\partial Q_{total} / \partial\, \dot{V}_{RA,CFM}$ = 3.197	0.07 %

Figure 6.3. Uncertainty results

Uncertainty analysis was performed using the measured inputs from February 1 to February 28. Figure 6.3 indicates that outside air temperature, outside air flow rate and return air temperature played an influential role in energy consumption.

7. CONTROL STRATEGY OPTIMIZATION

In baseline model, discharge air temperature was set at 55°F and supply air static pressure was set at 1.80 inch WC. In order to improve energy efficiency, discharge air temperature reset and supply air static pressure reset control strategies were applied. In cooling mode, increasing discharge air temperature reduces mechanical cooling energy and also terminal reheat. However, fan speed increases with a raise in discharge air temperature in order to compensate.

Supply air static pressure should be maintained just as high as it is required to satisfy the zone that needs most energy. The supply air static pressure and discharge air temperature reset control strategies interact with each other to compete for capacity control. Therefore, individual reset control strategy was evaluated separately.

7.1 Discharge Air Temperature Reset

Figure 7.1 shows the DA-T reset logic. The reset logic is direct proportional calculation on a RA-T input span of 70°F to 73°F and a DA-T output of 64°F to 56°F. The correlation between DA-T and RA-T is shown in Figure 7.2.

7.2 Static Pressure Reset

According to ASHRAE 90.1-2010, for systems with DDC of individual zone boxes reporting to the central control panel, static pressure setpoint shall be reset based on the zone requiring the most pressure; i.e., the setpoint is reset lower until one zone damper is nearly wide open.

Supply fan speed command was determined by the supply air static pressure. The speed was varied to maintain the set point of 1.80 inch WC. The static pressure was measured at 2/3 of the supply air ductwork. The AHU was running a high supply air

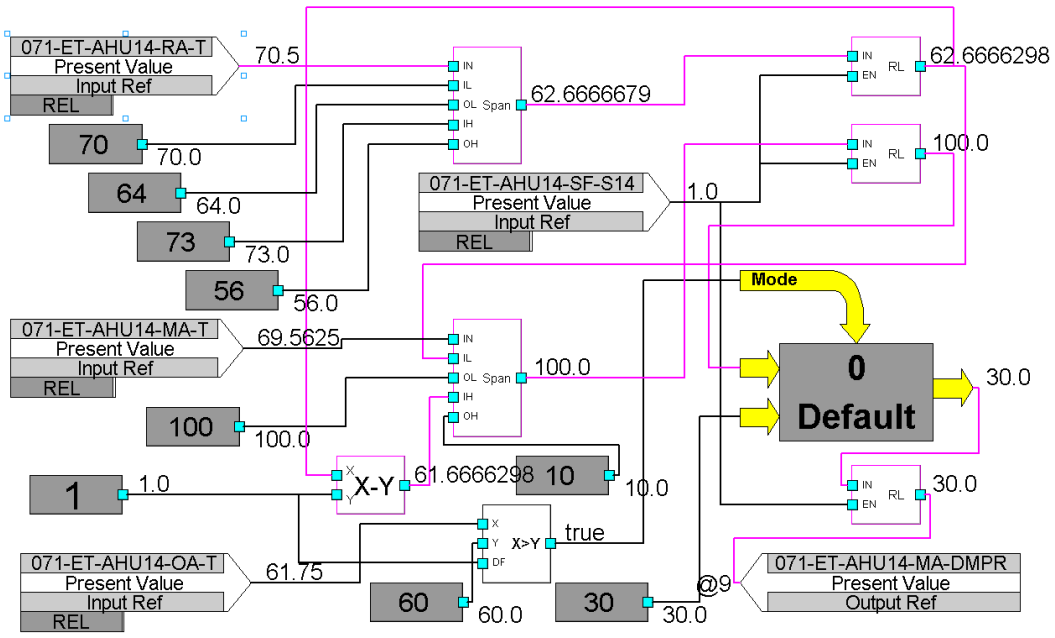

Figure 7.1. Discharge air temperature reset logic

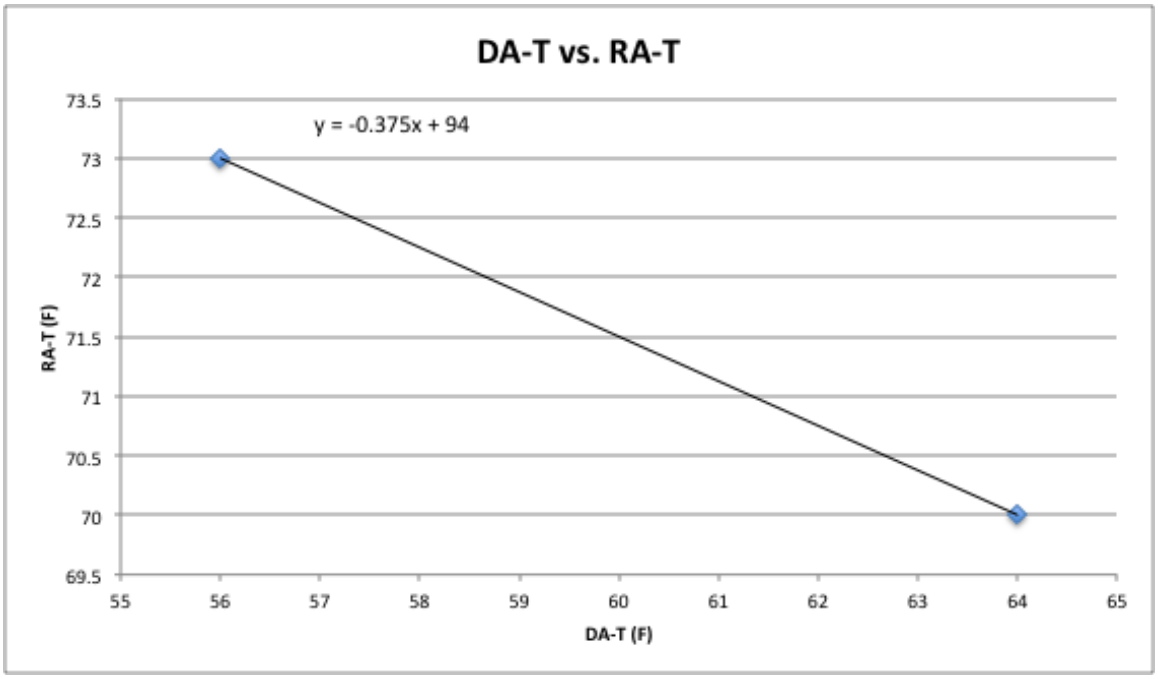

Figure 7.2. Correlation between DA-T and RA-T in DA-T reset logic

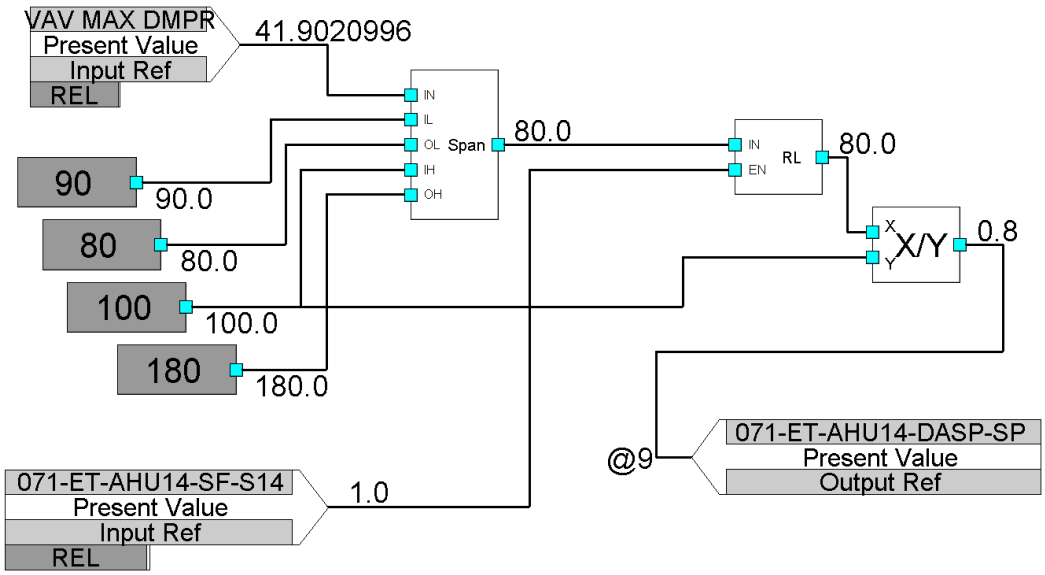

Figure 7.3. Supply air static pressure reset logic

static setpoint because of an initial problem satisfying the cooling needs of a server room. They now have an additional cooling supplied by an air conditioner.

Supply air static pressure reset control logic was applied to reduce energy consumption. The control logic is displayed in Figure 7.3. If one zone damper is greater than 90% then increase static pressure setpoint proportionally from the minimum of 0.8 inch WC to the previous maximum of 1.80 inch WC based on the damper range of 90% to 100%.

7.3 Potential Energy Saving Prediction

Baseline of energy consumption was calculated using the inputs collected from February 25 to February 28. Data was collected from March 4 to March 7 when applied discharge air temperature reset (control strategy 1). Data was collected from March 20 to March 23 when applied static pressure reset (control strategy 2).Description of data sets is shown in Table 7.1.

Table 7.1. Description of data sets for energy consumption comparison

Data Set No.	**Time Period**	**Sampling Time**	**NO. of Samples**	**Avg. OA-T**	**Avg. OA-H**
1	2/25/2015-2/28/2015	3.5 days	500	22°F	65%
2	3/4/2015-3/7/2015	3.5 days	500	27°F	68%
3	3/20/2015-3/23/2015	3.5 days	500	45°F	62%

Table 7.2. Energy savings comparison between DA-T reset and SP reset

	Baseline	**Control Strategy 1**		**Control Strategy 2**	
	No Reset	**DA-T Reset**	**Energy Savings**	**SP Reset**	**Energy Savings**
OA-T (°F)	22	27		45	
Q_rh (BTU)	9633080	7175178	2457902	8831474	801606
Q_cc (BTU)	0	0	0	144851	-144851
Q_hw (BTU)	130893	0	130893	11147	119746
E_SF (BTU)	1242296	1693561	-451265	1225516	16779
E_RF (BTU)	420964	597082	-176117	412272	8692
Q_total (BTU)	9633080	7175178	2457902	8831474	801606

Table 7.2 demonstrates that when the system utilized DA-T reset, the total energy consumption reduced by 17.2%. Reheat energy consumption decreased by 25.5%. Preheat coil energy savings were 130,893 BTU during the period that DA-T reset was applied. However, 100% closed preheat coil valve resulted from the higher outdoor air temperature but not the reset supply air temperature. Both supply fan and return fan power went up to compensate the decreased temperature difference.

When supply air static pressure setpoint was reset, the total energy consumption reduced by 7%. In particular, reheat energy consumption went down 8.3%. Cooling

energy increased because an increase in outdoor air temperature drove the cooling coil valve open. Supply fan power consumption decreased by 1.4% while return fan power consumption decreased by 2.1%.

Outside conditions were different when applied DA-T reset schedule and static pressure reset schedule, which might have an impact in the energy savings. When outside air temperature was between 45°F and 65°F, the unit was in economizer operation. The mixed air damper was modulated from minimum position to maximum position to provide free cooling. Supply fan ran faster to deliver more air.

8. DISCUSSIONS

At AHU level, individual component model was established using energy and mass balance governing equations. The theoretical model was then validated with two sets of real time data. The deviations of simulated results from measured data were identified through MAPE and RMSE.

The predicted outputs of mixing box model tended to have a lower accuracy when the ambient temperature was low. The possible reason could be that the outdoor air temperature sensor was not calibrated and it did not function well when operated in low temperature range. The second data set from March 1 to March 31 proved that the deviations from the measured data were much lower when the outdoor air temperature was above 40°F. The model performance of pre-heat coil and cooling coil were impacted by the accuracy of mixed air temperature since the mixed air temperature was an critical input to both pre-heat coil and cooling coil models.

The deviations of the fan models from measured data were greater compared to the other component models. The model performance of the fans varied with various fans. There is no one standard equation that is able to precisely predict the fan power consumption without knowing the actual fan performance curves.

The theoretical model could be used by Campus Facility Staff to predict potential energy savings when adopting a wide variety of measures under different operating conditions. It allows them to quantify and measure the improvements.

9. CONCLUSIONS AND RECOMMENDATIONS

9.1 Conclusion

The mathematical model was validated using two sets of sub hourly measured data from Metasys system. Generally speaking, the model performance is better when the ambient temperature is above 40°F.

The impact of input variables was identified in uncertainty propagation using RSS method. Outside air temperature, outside air flow rate and return air temperature were the most influential parameters in minimizing energy consumption.

Supply air static pressure reset and discharge air temperature reset strategies were good strategies to minimize the energy consumption. 17.2% energy savings was achieved using discharge air temperature reset while the energy consumption reduced by 7% using static pressure reset.

9.2 Recommendations for Future

Outside air humidity measurement

A humidity sensor can be added to the Metasys system to measure the outdoor air humidity.

Control system simulation and optimization

Control system simulation was not carried out in this project due to time restriction. Mixed air damper controller, cooling coil valve controller and pre-heat coil valve controller models can be integrated into the system model to better predict the system behaviors.

PID controllers can be optimized to stabilize the system operation. Advanced control of HVAC systems, such as Model Predictive Control (MPC), can be introduced in order to better optimize the system performance, enhance thermal comfort and reduce energy consumption.

Energy consumption metering

Heating and cooling energy metering is essential to identify the energy wastes at the early stage and validate the energy use reduction after conducting energy conserving techniques. Energy consumption is a function of water flow rate and temperature difference between entering water temperature and leaving water temperature. The chilled water and hot water flow rate measurements play a critical role in measuring the cooling and heating energy consumption [34, 35]. The pressure drop across the valve is able to be obtained by installing a differential pressure gauge on the cooling coil and pre-heat coil. The valve authority, flow coefficients and valve characteristics can be determined through a calibration process [34, 35]. Two temperature sensors can be installed on the supply water line and return water line for both cooling and heating coils for temperature measurements.

LIST OF REFERENCES

LIST OF REFERENCES

[1] Energy Information Administration, U.S. energy consumption, [Online]. Available: http://www.eia.gov/tools/faqs/faq.cfm?id=86&t=1 [Accessed: 26-Jun-2015].

[2] U.S. Department of Energy, Building energy data book, 2006.

[3] Energy Information Administration, EIA annual energy outlook, 2008.

[4] Varkie C. T, HVAC: Centrifugal chillers, [Online]. Available: http://energy-models.com/hvac-centrifugal-chillers [Accessed: 26-Jun-2015].

[5] G. Wang and L. Song, Air handling unit supply air temperature optimal control during economizer cycles, *Energy and Buildings*, vol. 49, pp. 310-316, 2012.

[6] J. Zhou and D. Claridge, PI tuning and robustness analysis for air handler discharge air temperature control, *Energy and Buildings*, vol. 44, pp. 1-6, 2012.

[7] M. Liu, J. Feng, Z. Wang, L. Wu, K. Zheng, and X. Pang, Impacts of static pressure reset on vav system air leakage, fan power and thermal energy-part 1: Theoretical model and simulation, 2011.

[8] B. Housholder, A study on static pressure reset and instability in variable air volume HVAC systems, Graduate Theses and Dissertations, Iowa State University, 2011.

[9] A. Afram and F. Janabi-Sharifi, Review of modeling methods for HVAC systems, *Applied Thermal Engineering*, vol. 67, no. 1-2, pp. 507-519, 2014.

[10] Investopedia.com, Definition of Black Box Model, [Online]. Available: http://www.investopedia.com/terms/b/blackbox.asp. [Accessed: 26-Jun-2015]

[11] S. Kalogirou, Artificial neural networks and genetic algorithms in energy applications in buildings, *Advances in Building Energy Research*, vol. 3, no. 1, pp. 83-119, 2009.

[12] S. Katipamula, T. Reddy and D. Claridge, Multivariate regression modeling, *J. Sol. Energy Eng.*, vol. 120, no. 3, p. 177, 1998.

[13] A. Kusiak, F. Tang and G. Xu, Multi-objective optimization of hvac system with an evolutionary computation algorithm. *Energy*, vol. 36, no. 5, pp. 2440-2449, 2011.

[14] Handbook-Fundamentals, American society of heating, refrigerating and air-conditioning engineers. Inc., *Inc., NE Atlanta, GA*, 2009.

[15] Softwaretestinggenius Inc. Comparison among black-box and white-box tests [Online]. Available:http://www.softwaretestinggenius.com/photos/wbtut1.JPG. [Accessed: 27-Jun-2015]

[16] B. Tashtoush, M. Molhim and M. Al-Rousan, Dynamic model of an HVAC system for control analysis, *Energy*, vol. 30, no. 10, pp. 1729-1745, 2005.

[17] A. Afram and F. Janabi-Sharifi, Gray-box modeling and validation of residential HVAC system for control system design, *Applied Energy*, vol. 137, pp. 134-150, 2015.

[18] T. Maile, M. Fischer, and V. Bazjanac. Building energy performance simulation tools-a life-cycle and interoperable perspective. *Center for Integrated Facility Engineering (CIFE) Working Paper*, 107:1–49, 2007.

[19] P. Li, Y. Li, J. Seem, H. Qiao, X. Li and J. Winkler, Recent advances in dynamic modeling of HVAC equipment. part 2: Modelica-based modeling, *HVAC&R Research*, vol. 20, no. 1, pp. 150-161, 2014.

[20] F-Chart Software, EES Engineering Equation Solver, [Online]. http://www.fchart.com/assets/downloads/ees_manual.pdf. [Accessed: 27-Jun-2015]

[21] BUREAU OF Facilities Programming & Utilization IU Bloomington, IUPUI Engineering Tech. Basement Floor Level 1 of 5, 2006.

[22] Moore Engineers, *IUPUI AHU-1 Schedules*, 2005.

[23] Titus HVAC, Digital single duct terminal, [Online].https://www.titus-hvac.com/Products/Terminal%20Units/DESV#. [Accessed: 27-Jun-2015]

[24] Johnson Controls, Metasys Building Automation System, [Online]. http://www.johnsoncontrols.com/content/us/en/products/metasys.html. [Accessed: 27-Jun-2015].

[25] Johnson Controls. Metasys system extended architecture overview technical bulletin. 2011.

[26] Johnson Controls, AHU-1 Sequence of Operation, 2006.

[27] Commissioninghvac, Diagram of the Mixing box, [Online].http://www.commissioninghvac.org/files/dlib/mixingbox.pdf. [Accessed: 10-Jun-2015].

[28] T. Mulumba, A. Afshari, K. Yan, W. Shen and L. Norford, Robust model-based fault diagnosis for air handling units, *Energy and Buildings*, vol. 86, pp. 698-707, 2015.

[29] K. V. Haperen. *Recommendations for calculations of energy consumption for air handling units*. EUROVENT, 2005.

[30] P. Salimifard, P. Delgoshaei, K. Xu, and J. D. Freihaut. Comparison of actual supply air fan performance data to ASHRAE 90.1 Standard-2010 and DOE commercial reference buildings part load fan energy use formula. ASHRAE/IBPSA-USA Building Simulation Conference, 2014.

[31] Carrier Corporation Air Handling Unit Product data New York,Syracuse, 2006.

[32] I. Zajic, T. Larkowski, M. Sumislawska, K. J. Burnham, and D. Hill, Modelling of an air handling unit: a hammerstein-bilinear model identification approach. In *Systems Engineering (ICSEng), 2011 21st International Conference on*, pp. 59–63. IEEE, 2011.

[33] Heat Transfer Solutions Inc., Heat transfer coefficients, [Online].http://www.hcheattransfer.com/coefficients.html. [Accessed: 10-Jun-2015].

[34] L. Song, A. Swamy, and G. Shim, Feasibility study of developing a virtual chilled water flow meter at air handling unit level,

[35] A. Swamy, L. Song, and G. Wang, A virtual chilled-water flow meter development at air handling unit level. *ASHRAE Transactions*, 118:1013, 2012. 2011.

[36] Y. Zhao, Variable Air Volume (VAV) air handling system what makes VAV box performance better, 2011.

[37] J. Frost. Regression analysis: How do I interpret R-squared and assess the goodness-of-fit? 2013.

[38] SAS Institute Inc., *Details of Model Selection*, [Online]. http://www.okstate.edu. [Accessed: 27-Jun-2015].

[39] R. Hyndman and A. Koehler, Another look at measures of forecast accuracy. *International Journal of Forecasting*, vol. 22, no. 4, pp. 679-688, 2006.

[40] S. Klein and G. Nellis, *Mastering EES*, Madison, WI: F-Chart Software, 2013.